Journal of Wind Engineering & Industrial Aerodynamics 170 (2017) 238–255

Contents lists available at ScienceDirect

Journal of Wind Engineering & Industrial Aerodynamics

journal homepage: www.elsevier.com/locate/jweia

Local-scale forcing effects on wind flows in an urban environment: Impact of geometrical simplifications

A. Ricci [a,b,*], I. Kalkman [b], B. Blocken [b,c], M. Burlando [a], A. Freda [a], M.P. Repetto [a]

[a] Department of Civil, Chemical and Environmental Engineering (DICCA), University of Genoa, Genoa, Italy
[b] Building Physics and Services, Department of the Built Environment, Eindhoven University of Technology, Eindhoven, The Netherlands
[c] Building Physics Section, Department of Civil Engineering, KU Leuven, Leuven, Belgium

ARTICLE INFO

Keywords:
CFD simulations
Urban wind flow
Model detailing
Geometric uncertainties
Statistical performance

ABSTRACT

Wind flow in urban areas is strongly affected by the urban geometry. In the last decades most of the geometries used to reproduce urban areas, both in wind-tunnel (WT) tests and Computational Fluid Dynamics (CFD) simulations, were simplified compared to reality in order to limit experimental effort and computational costs. However, it is unclear to which extent these geometrical simplifications can affect the reliability of the numerical and experimental results. The goal of this paper is to quantify the deviations caused by geometrical simplifications. The case under study is the district of Livorno city (Italy), called *"Quartiere La Venezia"*. The 3D steady Reynolds-averaged Navier-Stokes (RANS) simulations are solved, first for a single block of the district, then for the whole district. The CFD simulations are validated with WT tests at scale 1:300. Comparisons are made of mean wind velocity profiles between WT tests and CFD simulations, and the agreement is quantified using four validation metrics (*FB*, *NMSE*, *R* and *FAC1.3*). The results show that the most detailed geometry provides improved performance, especially for wind direction $\alpha = 240°$ (22% difference in terms of *FAC1.3*).

1. Introduction

The complex morphology of cities renders the analytical description of wind flow in urban areas very difficult. Analytical wind flow models are generally well established over flat open terrain, where the wind profiles mainly depend on the aerodynamic roughness of the surface and on thermal stratification. In contrast, wind flow in urban environments is governed by a variety of complex factors, such as the heterogeneous geometry of buildings, flow impingement, separation and recirculation and local thermal effects.

The region above the buildings, usually defined as the urban boundary layer (UBL), is influenced by continuously changing surface roughness, so that the wind flow never reaches a homogeneous equilibrium condition. The situation is even more complex within the urban canopy layer (UCL), where streets give rise to complex canyoning effects that are strongly dependent on the canyon orientation with respect to the incoming wind. Many researchers have investigated different aspects of urban flows (see e.g. reviews by Britter and Hanna, 2003; Fernando, 2010; Fernando et al., 2010), but at present the UBL is not yet completely understood although WT tests and CFD simulations are frequently used in urban physics and wind engineering to gain increased understanding.

In the last decades, several studies have focused on numerical modeling of wind flow over random urban-like obstacles (e.g. Xie et al., 2008), uniform and staggered building arrays (e.g. Coceal and Belcher, 2004; Xie and Castro, 2006; An et al., 2013; Razak et al., 2013), idealized urban surfaces (e.g. Cheng and Porté-Agel, 2015), semi-idealized urban canopies (e.g. Hertwig et al., 2012) and actual urban environments (Blocken et al., 2012; Janssen et al., 2013; Montazeri et al., 2013; García Sánchez et al., 2014). Errors and uncertainties can be related to the geometrical model precision, the approximate form of the governing equations (RANS, LES), the turbulence models, the discretization schemes and the boundary conditions such as the inflow conditions and the surface roughness (Franke et al., 2007; Blocken et al., 2007a; Hargreaves and Wright, 2007; Tominaga et al., 2008a, b; Emory et al., 2013; Gorlé et al., 2015). Carpentieri and Robins (2015) analyzed the impact of morphological parameters on wind flow in the UCL. Their results show how the building height variability, the angles between street canyon orientations and incoming wind and other local geometrical features can strongly influence the characteristics of the urban flow.

Several authors (Chang and Meroney, 2003; Fernando, 2010; Barlow,

* Corresponding author. Department of Civil, Chemical and Environmental Engineering (DICCA), University of Genoa, Genoa, Italy.
E-mail addresses: alessio.ricci@unige.it, a.ricci@tue.nl (A. Ricci), i.m.kalkman@tue.nl (I. Kalkman), b.j.e.blocken@tue.nl, bert.blocken@kuleuven.be (B. Blocken), massimiliano.burlando@unige.it (M. Burlando), andrea.freda@unige.it (A. Freda), repetto@dicca.unige.it (M.P. Repetto).

http://dx.doi.org/10.1016/j.jweia.2017.08.001
Received 14 September 2016; Received in revised form 20 July 2017; Accepted 5 August 2017
Available online 28 September 2017

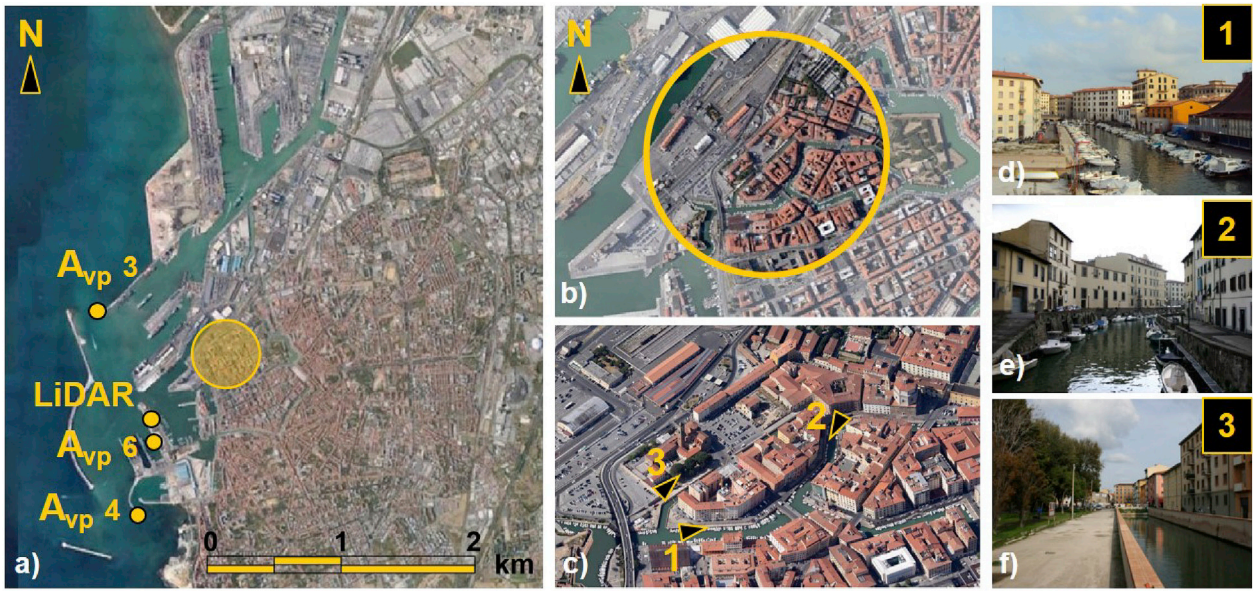

Fig. 1. Pictures of Livorno city (Italy): (a) location of the test district (yellow circle), anemometric stations (A_{vp} 3, A_{vp} 4 and A_{vp} 6) and LiDAR station, (b–c) test district *Quartiere La Venezia*, (d) *Canale Rosciano* (West – East), (e) *Canale Rosciano* (Northeast – Southwest), (f) a small canal inside *Quartiere La Venezia*. (For interpretation of the references to colour in this figure legend, the reader is referred to the web version of this article.)

2013) stressed that the complexity of the UBL requires studies with multiple approaches with complementary strengths and weaknesses. In particular, the joint use of WT testing and CFD simulations has enabled a better understanding of urban aerodynamics and has enhanced the performance of both (Murakami, 1990; Stathopoulos, 1997; Baker, 2007; Tominaga and Stathopoulos, 2013, 2016; Blocken, 2014, 2015; Meroney, 2016). However, results of both techniques are strongly dependent on geometrical model details (AIAA, 1998; Casey and Wintergerste, 2000; AIJ, 2004; Franke, 2006; Blocken, 2014). Nevertheless, geometrical simplifications are frequently adopted and often even required in both techniques, and the question therefore arises to what extent different levels of geometrical simplification can affect the results.

The aim of this study is to quantify the so-called *uncertainty* (AIAA, 1998; Oberkampf et al., 2004; Versteeg and Malalasekera, 2007) caused by geometrical simplifications of the urban model, both intentionally imposed (e.g. to limit experimental manufacturing cost or computational cost) and arising from a limited knowledge of the system to be analyzed (e.g. the epistemic uncertainty). For this purpose, a historical district called *"Quartiere La Venezia"* in Livorno city (Italy) is selected as case study. This area is chosen because the nearby port has been monitored by different measurement instruments in several locations, which will provide input data for the present study. They consist of anemometric stations and a LiDAR wind profiler installed in the framework of the European projects *"Wind and Ports"* (Solari et al., 2012) and *"Wind, Ports, and Sea"* (Burlando et al., 2015a; Repetto et al., 2017). The location is particularly interesting since the highest wind velocity observations generally occur for Western winds, in which case the incoming velocity profile in the district can be measured by the aforementioned LiDAR station (Fig. 1). Moreover, the transition from sea to land is expected to strongly influence the vertical wind profile in this area. WT tests on a model of the district at scale 1:300 were performed and reported in an earlier study (Ricci et al., 2017).

In the present paper, 3D steady-state RANS simulations using the realizable k-ε turbulence model are performed at the same scale as the WT tests in two different steps. First, CFD simulations are performed on a single block of *Quartiere La Venezia* with three different levels of geometrical simplification, i.e. the so-called *simplified*, *approximated* and *detailed* geometrical models, where the latter has an identical geometry as

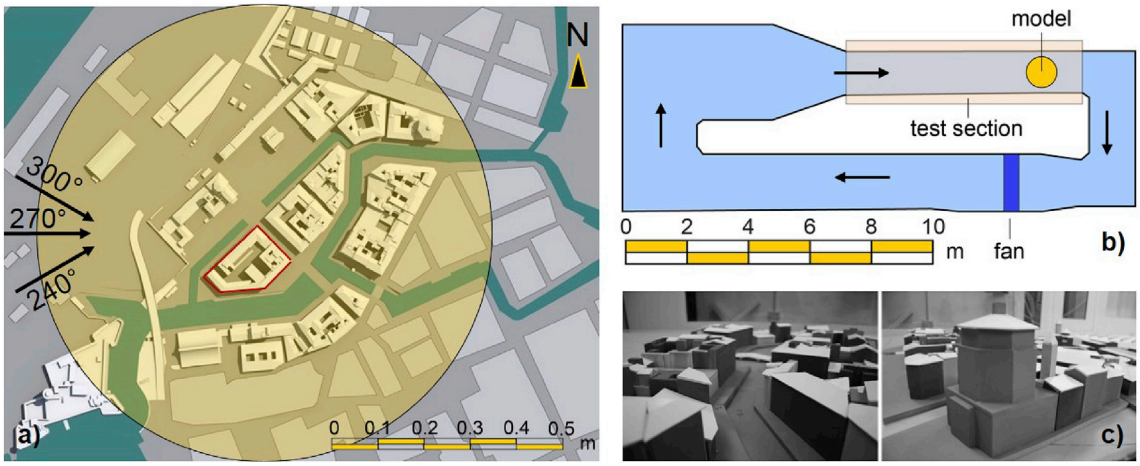

Fig. 2. Wind-tunnel experiments: (a) digital model used to build the WT model, (b) WT schematic, (c) pictures of the WT model. Only the buildings shown as extruded volumes in Fig. 2a were included in the WT model. The red outline indicates the group of buildings simulated in the first step (single block; Section 3). (For interpretation of the references to colour in this figure legend, the reader is referred to the web version of this article.)

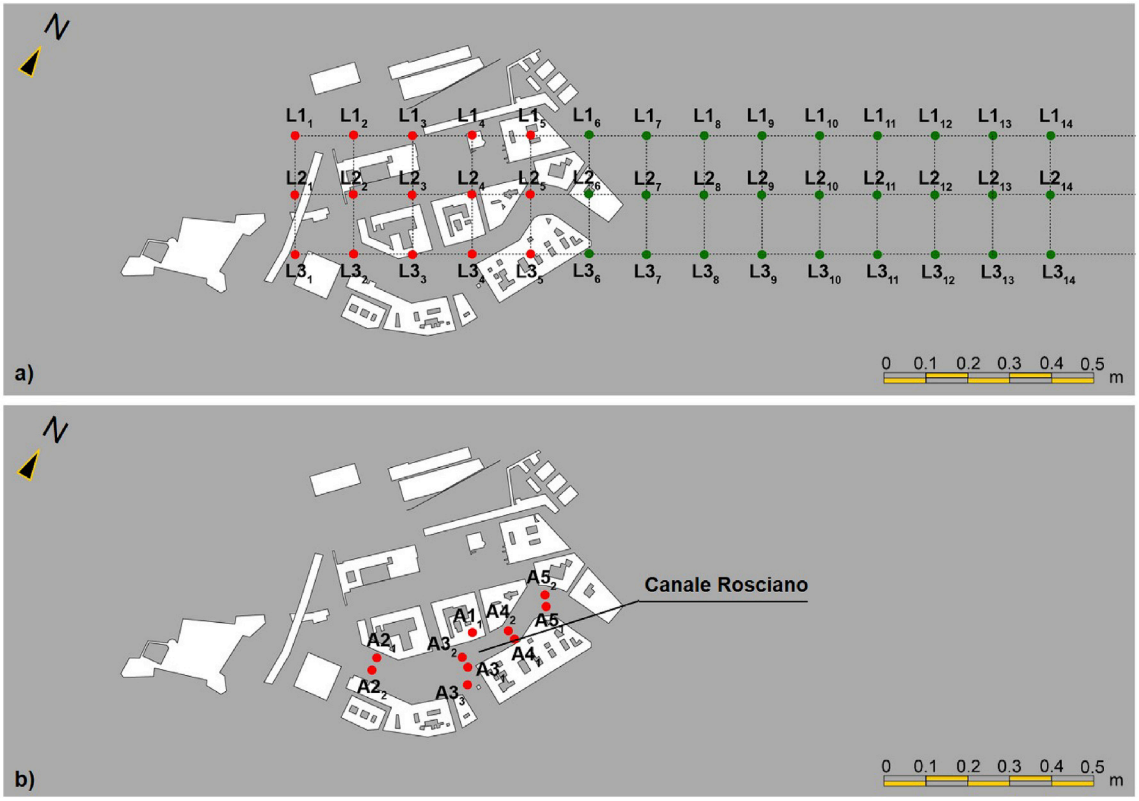

Fig. 3. Location of measurement positions (a) ($L1_{1\text{-}14}$, $L2_{1\text{-}14}$, $L3_{1\text{-}14}$) and (b) ($A1_1$-$A5_2$) in the investigated district of Livorno city. The red positions were used for comparison of WT and CFD results (Section 4.2.2). The green positions were only used to compare the results of two CFD models (Section 4.2.2). (For interpretation of the references to colour in this figure legend, the reader is referred to the web version of this article.)

the WT model. Second, simulations are performed for the whole urban model of *Quartiere La Venezia* for two of the three levels of geometrical simplification, i.e. the *simplified* and the *approximated* geometrical models.

The paper is organized as follows. Section 2 contains a short description of the WT tests used to validate the CFD simulations. Section 3 and Section 4 describe two steps of CFD analysis. In particular, Section 3 introduces the CFD models (*simplified*, *approximated* and *detailed*), the boundary conditions and the computational setup for the simulations for the single block of *Quartiere La Venezia*. On the basis of the obtained results, Section 4 describes the CFD simulations for the whole urban district adopting the *simplified* and *approximated* models, and shows the comparison of the WT and CFD results in terms of mean velocity profiles. In Section 5, the level of agreement between WT and CFD results is quantified using validation metrics. Finally, Section 6 (discussion and limitations) and Section 7 (summary and conclusions) conclude the paper.

2. Description of the wind-tunnel experiments

Only some main aspects of the WT tests are mentioned in this section; the reader is referred to Ricci et al. (2017) for more details. WT tests on a geometrical model of the whole urban district were performed in the atmospheric boundary layer (ABL) wind tunnel of the Department of Civil, Chemical and Environmental Engineering (DICCA) of the Polytechnic School of the University of Genoa, Italy. The wind tunnel at DICCA is a closed-loop subsonic circuit with a test section of 8.8 m long and a cross-section of 1.70 m (width) x 1.35 m (height) (Fig. 2b). A WT model of the case study - *Quartiere la Venezia* in Livorno city - was created at a scale of 1:300 using medium density fiberboard (MDF) of different thicknesses for the ground plates and buildings, and 3 mm closed cell PVC foamboard panels for roofs and bridges (Fig. 2a,c). The blockage ratio in the cross-section was kept below 3.5% for all wind directions. Tests were performed for three western wind directions ($\alpha = 240°$, 270° and 300°), corresponding to the prevalent wind directions for the strongest winds in Livorno (Fig. 2a). The mean wind velocity scenarios obtained during the European project *"Wind and Ports"* (Solari et al., 2012) by means of the WINDS model (Wind Interpolation by Non-Divergent Schemes), anemometric data, and the digital land cover maps of the CORINE project (Bossard et al., 2000) were used as reference for the choice of the incoming flow profiles in the WT tests. Based on this, an ABL profile with aerodynamic roughness length $z_0 = 0.1$ m (full scale) and friction velocity $u^* = 0.89$ m/s was used for the WT tests.

In the WT tests, the mean wind velocity was measured at two sets of positions (Fig. 3). In the first set, 10 positions inside *"Canale Rosciano"* ($A1_1$ - $A5_2$) were monitored at 15 heights in the range from 0.02 to 0.6 m above the wind-tunnel floor (corresponding to 6 m and 180 m full scale above mean sea level). Since these positions are fixed to the model geometry, their position in the WT is dependent on model orientation and hence on wind direction. The second set was distributed along a Cartesian grid laid out according to the WT local reference system, consisting of 15 measurement locations at 15 heights (from 0.02 to 0.6 m above the wind tunnel floor) aligned along three lines of five measurement positions each ($L1_{1\text{-}5}$, $L2_{1\text{-}5}$, $L3_{1\text{-}5}$). Both sets of measurements will be used to validate the CFD simulations performed on the urban district, *Quartiere La Venezia*, described in Section 4. A third set of measuring positions ($L1_{6\text{-}14}$, $L2_{6\text{-}14}$, $L3_{6\text{-}14}$), indicated in Fig. 3 by the green points, was used to investigate the wind velocity profile development in the downstream part of the computational domain. The results of this investigation are described in Section 4.

3. CFD simulations of a single block of Quartiere La Venezia

3.1. Computational geometry, domain and grid

In the first step, CFD simulations were performed on a single block of

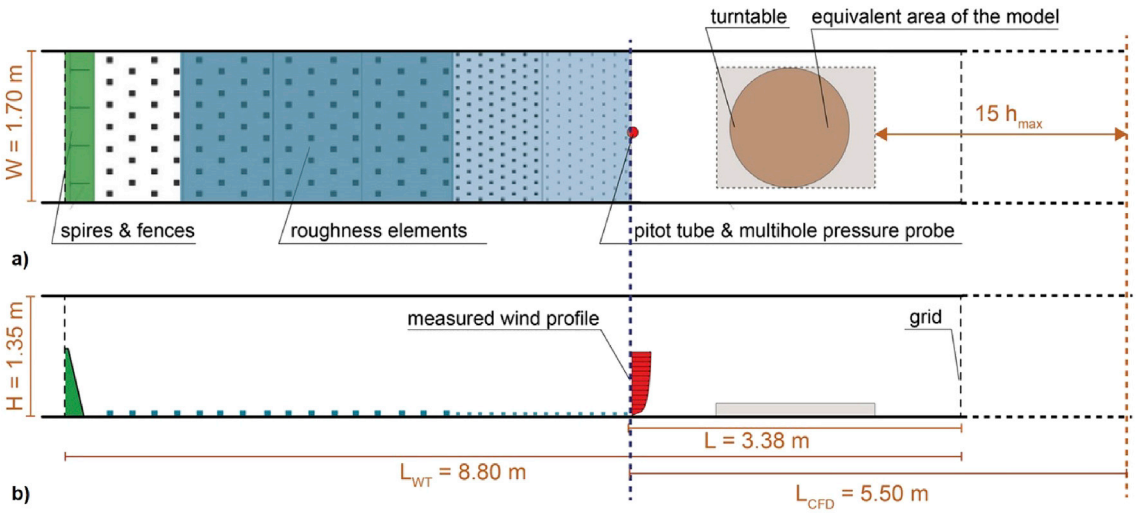

Fig. 4. Relationship between the WT test-section and the CFD computational domain: (a) top view and (b) side view of wind-tunnel test section. Symbols: (W) width and (H) height of the WT and computational domain; (L_{WT}) length of the test section; (L) distance between the position of the measured wind profile and the end boundary; (L_{CFD}) length of the computational domain; ($15\ h_{max}$) distance between the last building of the urban model and the outlet face of the computational domain, where h_{max} is the maximum building height.

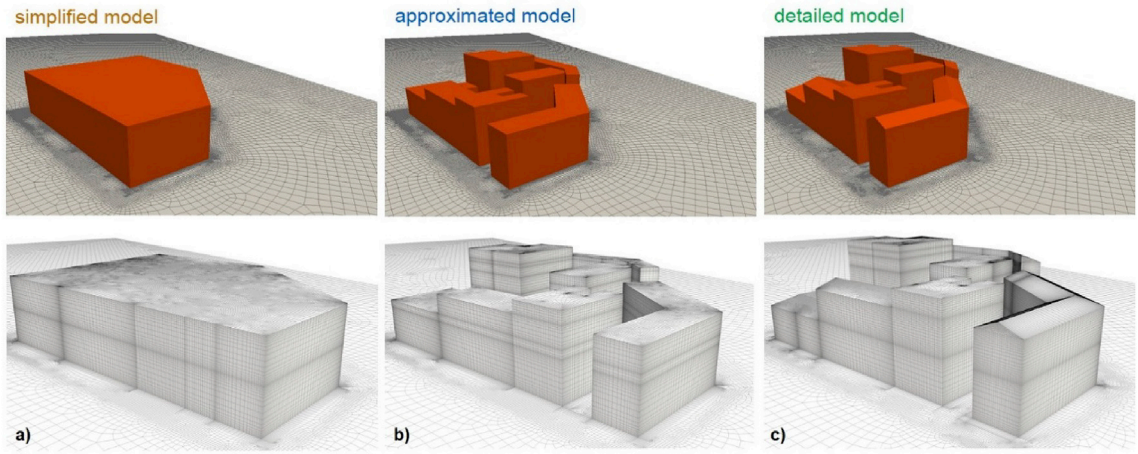

Fig. 5. Geometry and computational grid on building and ground surfaces for (a) *simplified*, (b) *approximated*, (c) *detailed* geometrical models of a block of buildings of *Quartiere La Venezia*, for the wind direction $\alpha = 240°$. The selected group of buildings is indicated by a red outline in Fig. 2a. (For interpretation of the references to colour in this figure legend, the reader is referred to the web version of this article.)

Quartiere La Venezia (indicated by the red outline in Fig. 2a) at the same scale of the WT tests (1:300) and for wind direction $\alpha = 240°$, in order to preliminarily investigate the deviations caused by three different levels of geometrical simplification (i.e. called hereafter *simplified*, *approximated* and *detailed* geometrical models). Based on the CFD results obtained in this step, the criteria to realize the geometries of the whole urban district were chosen for the second step. Fig. 4 shows the relationship between the WT test-section and the CFD computational domain. The size of the computational domain was $L \times W \times H = 5.5 \times 1.70 \times 1.35\ m^3$, where the width ($W$) and height ($H$) are coincident with the WT cross-section. The three CFD geometrical models and the associated grids were realized using the software Gambit 2.4.6. The first one, termed *simplified* geometrical model, was obtained representing the single group of buildings as a single bluff body with a height equal to the arithmetic average height of that building group (Fig. 5a). The second one, termed *approximated* geometrical model, was obtained including buildings with their real ground plan and heights, but replacing pitched roofs with flat ones (Fig. 5b). To this purpose, the height of every building was calculated as the average between the heights of the peak and the eaves of the pitched roofs. Note that the pitch of the roofs of *Quartiere La Venezia* are probably less relevant from the aerodynamic point of view, since these are low-sloped roofs with slopes in the range of only about 5°–10°.

The third one, the *detailed* geometrical model, was perfectly coincident with the WT geometrical model, including the real ground plan and heights of the buildings including pitched roofs (Fig. 5c). Grid generation for the simplified and approximated geometrical was performed using the surface grid generation technique presented by van Hooff and Blocken (2010) in order to achieve a high-level control over the grid layout. Grid generation for the detailed geometrical model was performed only in part using this technique due to the sloped roof geometry. All three grids were constructing adhering to the best guidelines (Franke et al., 2007; Tominaga et al., 2008a; Blocken, 2015). The local grid resolution was taken equal or higher than that in previous studies that used the same technique and employed certain grid resolutions based on detailed grid-sensitivity tests (van Hooff and Blocken, 2010; Blocken et al., 2012). The expansion ratio of the grid was kept below 1.2 everywhere in the computational domain and at least thirty cells were used along every building edge, which is far beyond the minimum number of ten mentioned in the best practice guidelines (Franke et al., 2007; Tominaga et al., 2008a). In order to avoid convergence problems and maximize numerical accuracy, only hexahedral and prismatic cells were

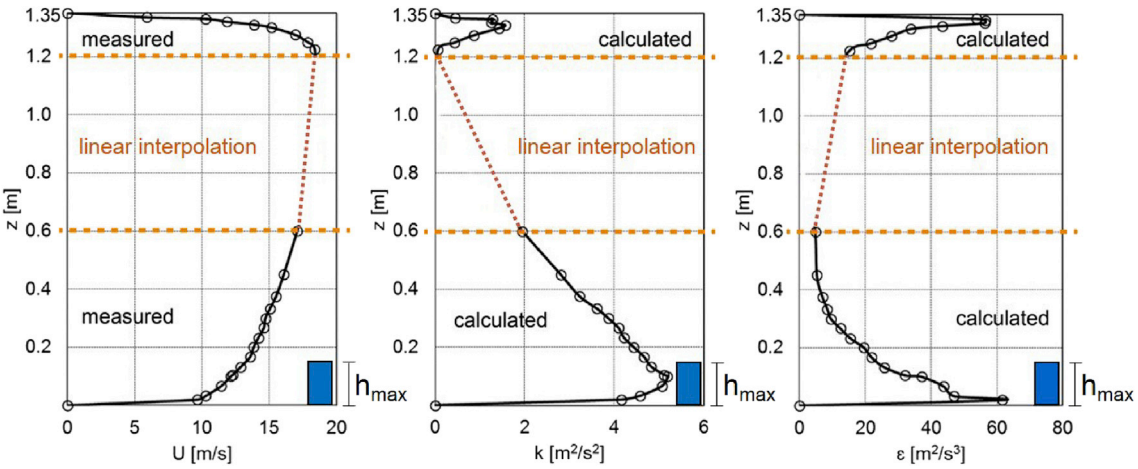

Fig. 6. Inlet profiles: mean wind velocity (U), turbulent kinetic energy (k) and turbulence dissipation rate (ε). Also indicated are measured values (black circles). The height of the tallest building (h_{max}), as indicated by the blue rectangle in the figure, is equal to 0.15 m (corresponding to 45 m full scale). (For interpretation of the references to colour in this figure legend, the reader is referred to the web version of this article.)

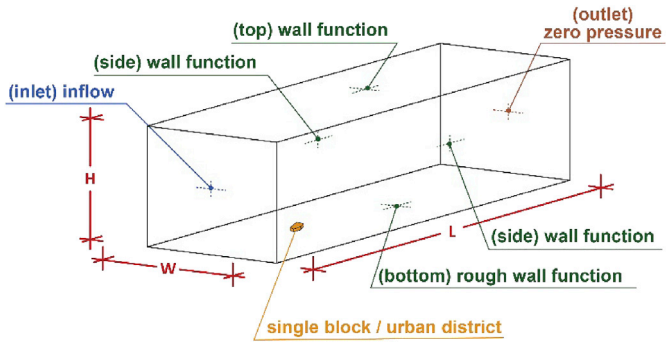

Fig. 7. Boundary conditions for the computational domain.

used for the *simplified* and *approximated* geometrical models in line with van Hooff and Blocken (2010); conversely, hexahedral, prismatic and tetrahedral cells were employed in the *detailed* model because of the pitched roof geometries. The construction of the computational grid of the *detailed* geometrical model was found to be about five times more computationally demanding (user time and processing time combined) than the other two geometrical models. The resulting grids counted 5.9 million cells for the *simplified* geometrical model, 8.5 million cells for the *approximated* geometrical *model*, and 11.8 million cells for the *detailed* geometrical model.

3.2. Boundary conditions

In order to reproduce the inflow conditions of the WT tests as accurately as possible, the inlet face of the computational domain was placed where the approach-flow profile was measured in the WT, that is approximately 1 m upstream of the first building of the urban model (Fig. 4). Hence, the measured vertical mean velocity profile was prescribed, and the vertical profiles of the turbulent kinetic energy $k(z)$ and the turbulence dissipation rate $\varepsilon(z)$ were calculated using the equations below (Tominaga et al., 2008a):

$$k(z) = \frac{1}{2}\left(\sigma_u^2(z) + \sigma_v^2(z) + \sigma_w^2(z)\right) \quad (1)$$

$$\varepsilon(z) = C_\mu^{0.5} k(z) \frac{dU}{dz} \quad (2)$$

For Eq. (1) the velocity standard deviations $\sigma_u(z)$, $\sigma_v(z)$ and $\sigma_w(z)$ measured in the WT tests were employed. In Eq. (2) the constant C_μ is 0.09 and a smoothing function was used to remove excessive numerical noise introduced by the gradient calculation. Since the WT equipment does not allow measurements to be made over the entire height of the WT cross-section, mean wind velocity and velocity standard deviations were directly measured only from 0 to 0.6 m and from 1.20 to 1.35 m. In the central part, between 0.6 and 1.20 m, these quantities were linearly interpolated in order to link both measured parts (Fig. 6). Note that the height of the tallest building is 0.15 m (corresponding to 45 m full scale) and as a result the particular shape of the vertical profiles above 0.6 m is expected to be of minor to no importance for the resulting flow patterns below the 0.15 m threshold.

At the bottom, sides and top of the domain as well as on the building and bridge surfaces, the standard wall functions by Launder and Spalding (1974) with roughness modification by Cecebi and Bradshaw (1977) were employed. At the bottom of the computational domain, an equivalent sand-grain roughness height k_s equal to 0.0013 m (0.39 m full scale) was imposed. This value was calculated in accordance with Blocken et al. (2007a) as $k_s = 9.793\, z_0/C_s$, where C_s (the roughness constant) was taken equal to 2.5 in order to comply with the necessary condition $y_p > k_s$, where y_p is the distance of the centroid of the first cell from the wall. The size of the first near-wall cell was chosen in order to obtain dimensionless wall unit values y^+ in the logarithmic layer range, i.e. 30–300 (Blocken et al., 2007a,b). An overview of these boundary conditions is given in Fig. 7. At the sides and top of the domain as well as on the building and bridge surfaces, k_s was equal to zero. At the outlet of the domain, zero static gauge pressure was imposed.

3.3. Solver settings

The CFD simulations were performed using the open-source CFD code OpenFOAM 2.3.0 with the 3D steady-state Reynolds-Averaged Navier-Stokes (RANS) approach. The *realizable* k-ε turbulence model was adopted for closure (Shih et al., 1995). Second-order discretization schemes were used for the convective and viscous terms of the governing equations. The SIMPLE algorithm was adopted to couple pressure and velocity fields (Patankar, 1980; Ferziger and Perić, 2002). Numerical convergence was achieved when the residuals showed no discernible fluctuation and further decrease during the iterative process. All CFD simulations were performed on a High Performance Computing (HPC) system at DICCA, using a computer node with 32 cores running in parallel at 1.4 GHz.

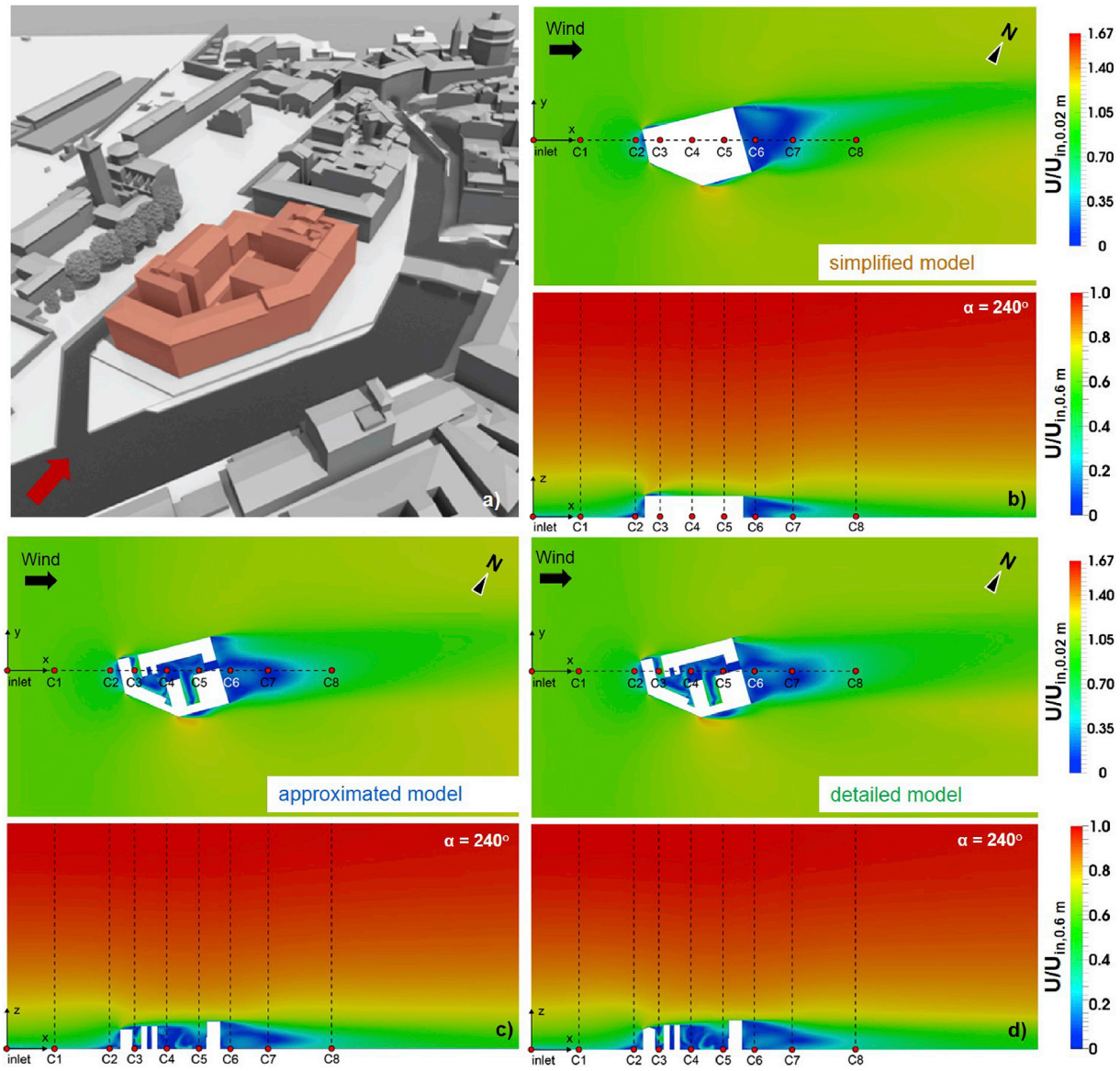

Fig. 8. (a) Perspective view of the selected single block of *Quartiere La Venezia* and nearby surroundings. Contours of amplification factor in horizontal and vertical plane for (b) *simplified*, (c) *approximated* and (d) *detailed* geometrical models, for wind direction $\alpha = 240^{\circ}$, made at 0.02 m above sea level (6 m full scale) and in a vertical centerplane of the computational domain (see Fig. 3a).

3.4. CFD results: comparison of results for the three geometrical models

The amplification factor $U/U_{in,0.02m}$ is defined as the local wind speed divided by the inlet wind speed at height $z = 0.02$ m ($U_{in,0.02m}$). The amplification factor $U/U_{in,0.60m}$ is defined in the same way but with inlet wind speed at height $z = 0.60$ m. Fig. 8 shows contours of the amplification factor in a horizontal plane at 0.02 m and in the vertical centerplane through L2 (see Fig. 3a). The CFD results for the three geometrical models exhibit almost the same wind-flow patterns upstream of the building block, both in terms of horizontal and vertical contours (Fig. 8). In contrast, significant differences are observed for the *approximated* and *detailed* geometrical models, with respect to the *simplified* one, at the courtyard and in the wake (Fig. 8c and d). The differences can be investigated more in detail by the mean wind velocity profiles at the positions C1 - C8 (Fig. 9). In Fig. 9, the axes show the ratio $U/U_{in,0.6m}$ (abscissa) vs. normalized reference height z/z_{ref} (ordinate), with reference height $z_{ref} = 0.60$ m. The deviations of the *simplified* and *approximated* geometrical models with respect to the *detailed* geometrical model are calculated in terms of differences between mean velocity ratios, $U/U_{in,0.6}$, i.e. $\Delta_{sim} = U_{sim}/U_{in,0.6} - U_{det}/U_{in,0.6}$ and $\Delta_{app} = U_{app}/U_{in,0.6} - U_{det}/U_{in,0.6}$, at the positions C1 - C8 and for four different levels (0.05, 0.1, 0.15 and 0.2 of z/z_{ref}) above the bottom of the domain (Table 1).

In general, the CFD results from the three geometrical models show the same wind velocity values above $z/z_{ref} \approx 0.2$. In contrast, the *approximated* and *detailed* geometrical models exhibit significant differences with respect to the *simplified* geometrical model (below $z/z_{ref} \approx 0.2$) at all positions except for C1 and C2 (upstream of the obstacle).

In the central part of the computational domain, at positions C3, C4 and C5, larger differences in terms of mean velocity ratio are found between the three CFD models mostly inside the courtyards of the buildings (for the *approximated* and *detailed* geometrical models). The *approximated* model shows small overestimations at positions C3 and C4 below $z/z_{ref} \approx 0.1$ with respect to the *detailed* model (Table 1). Below $z/z_{ref} \approx 0.1$, the *simplified* model evidently does not provide any velocity values due to the absence of the courtyards (Fig. 9 and Table 1). At $z/z_{ref} = 0.15$ and at $z/z_{ref} = 0.2$, the Δ_{app} values are smaller than Δ_{sim} (Table 1). Approximately the same trend of mean velocity ratio observed at positions C3 and C4 is also found at position C5 at levels 0.15 and 0.2 of z/z_{ref} (Table 1).

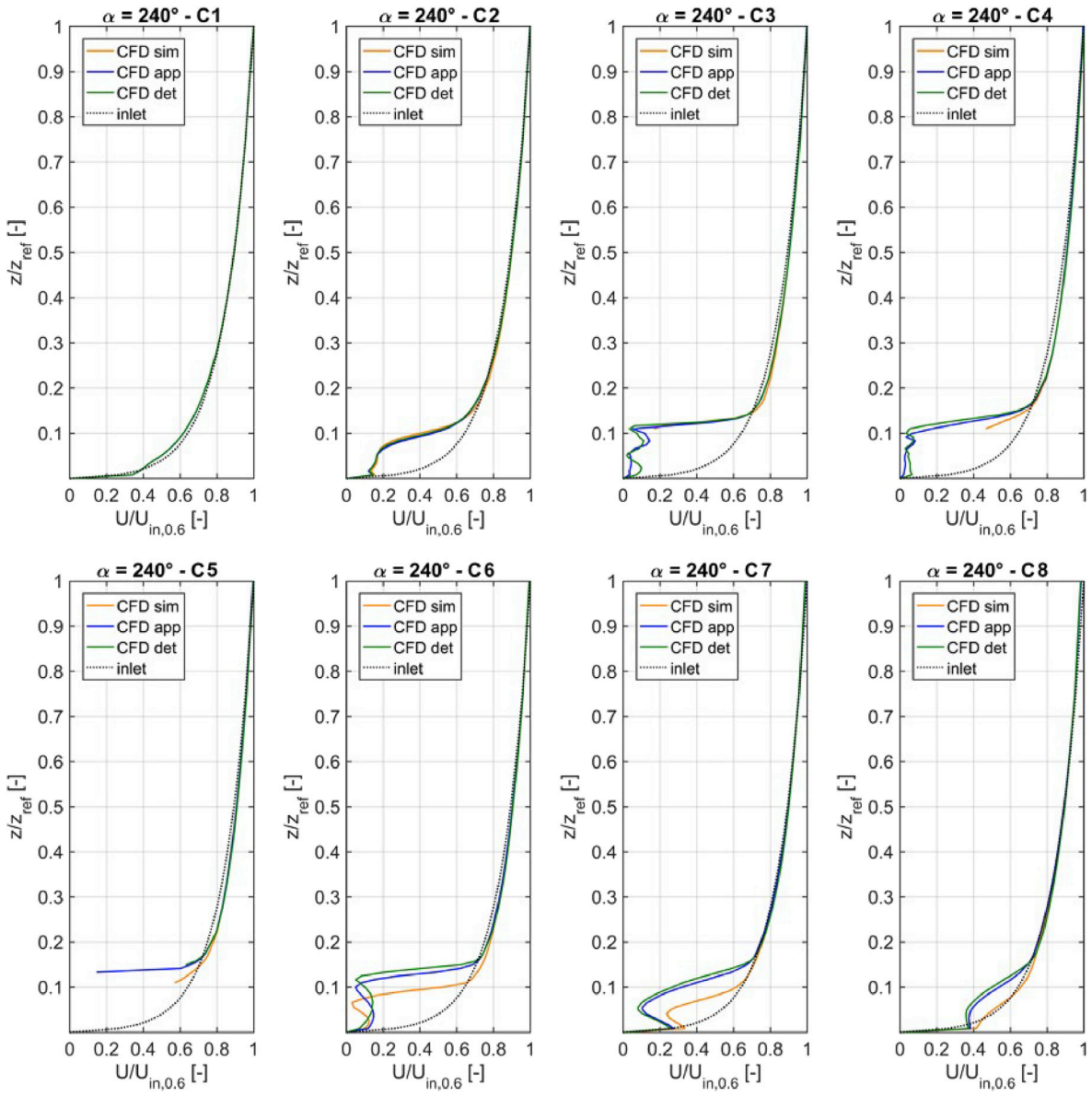

Fig. 9. Comparison of the vertical mean wind velocity profiles ($z_{ref} = 0.60$ m) above the points C1 - C8 for the inlet direction $\alpha = 240°$, for the *simplified* (CFD sim), *approximated* (CFD app) and *detailed* (CFD det) geometrical models. The inlet profile (black dashed line) is also shown for comparison.

Table 1
Variation in mean velocity ratio between *simplified* and *detailed models* (Δ_{sim}), and *approximated* and *detailed* geometrical models (Δ_{app}) at positions C1 - C8 (see Fig. 8).

z/z_{ref}	C1		C2		C3		C4	
	Δ_{sim}	Δ_{app}	Δ_{sim}	Δ_{app}	Δ_{sim}	Δ_{app}	Δ_{sim}	Δ_{app}
0.05	0	0.001	0.005	0.002	building	0.018	building	−0.017
0.1	0	0.001	−0.045	0.028	building	0.044	building	0.033
0.15	0	0.001	0.015	0.003	0.015	0.001	0.048	0.014
0.20	0.001	0.000	0.012	0.002	0.011	0.001	0.005	0.002
z/z_{ref}	C5		C6		C7		C8	
	Δ_{sim}	Δ_{app}	Δ_{sim}	Δ_{app}	Δ_{sim}	Δ_{app}	Δ_{sim}	Δ_{app}
0.05	building	building	−0.078	0.003	0.177	0.025	0.142	0.023
0.1	building	building	0.418	−0.052	0.348	0.052	0.158	0.040
0.15	0.082	0.027	0.117	0.066	0.060	0.021	0.034	0.004
0.20	0.003	−0.001	0.004	−0.005	0.000	−0.009	−0.008	−0.014

In the downstream part of the computational domain, at positions C6, C7 and C8, very substantial discrepancies in mean velocity ratio are found between the *simplified* and the other geometrical models (Fig. 9 and Table 1). A flattening of the three curves is observed at the positions C6 and C7 between 0.05 and 0.15 of z/z_{ref}, which increases with decreasing height of the buildings (Fig. 9). As a matter of fact, in the

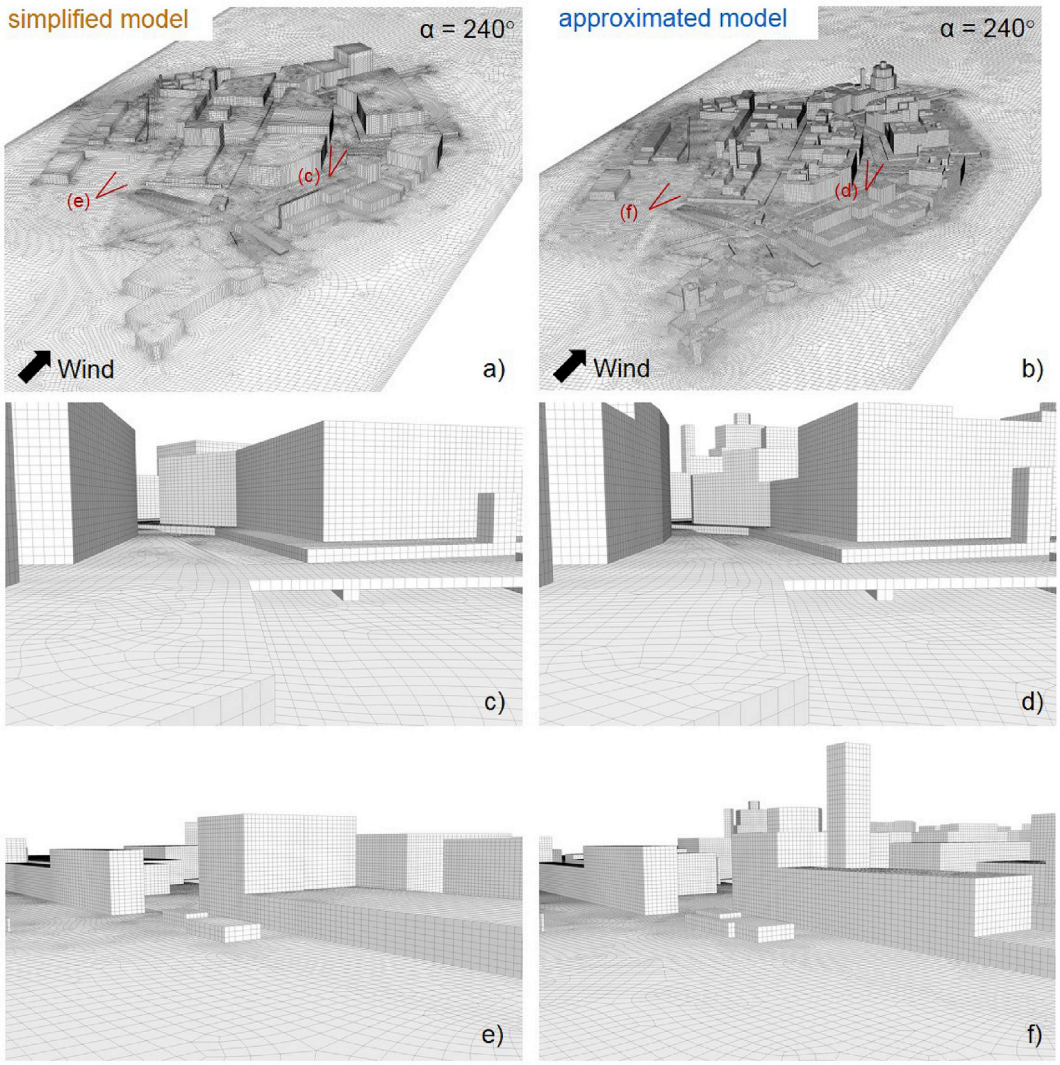

Fig. 10. Views of computational grid for (a,c,e) *simplified* and (b,d,f) *approximated* geometrical models of *Quartiere La Venezia* for the wind direction α = 240°.

simplified model the height of the single block (constant and equal to 0.07 m) is lower compared to the tallest building of the *approximated* and *detailed* models, respectively equal to 0.09 and 0.098 m. The results are clearly confirmed by the corresponding values of Δ_{sim} and Δ_{app} reported in Table 1.

Overall, a satisfactory agreement is found, in terms of velocity values, between the *approximated* and *detailed* models. Conversely, the *simplified* model shows large discrepancies with respect to both finer models at about all central and downstream positions.

Based on the satisfactory agreement between the *approximated* and *detailed* geometrical models, and considering that the construction of the *detailed* model is found to be about 5 times more computationally demanding (user time and processing time combined) than the *approximated* model, only the *simplified* and *approximated* models are retained for further study and are applied to the whole urban district *Quartiere La Venezia*.

4. CFD simulations of the urban district Quartiere La Venezia

4.1. Computational setup

In this second step, CFD simulations are performed on two geometries with different level of precision of the urban district *Quartiere La Venezia*, i.e. the *simplified* and *approximated* geometrical models. A computational domain with the same size (L x W x $H = 5.5 \times 1.70 \times 1.35$ m^3) as the one used in the first step (Section 3) is employed also in the current step. As already discussed in Section 3, since the grid generation is computationally demanding, a detailed grid-sensitivity analysis for each computational model and domain is not performed. However, in order to provide grid independent results, a very high-resolution of the grids is adopted based on the previous similar works published by van Hooff and Blocken (2010), Blocken et al. (2012) and Janssen et al. (2013) that are based on a detailed grid-sensitivity analysis. The computational grids are constructed using the surface-grid extrusion technique presented by van Hooff and Blocken (2010) in order to achieve a high-level of control over the grid and to adhere to the best guidelines (Franke et al., 2007; Tominaga et al., 2008a; Blocken, 2015). The expansion ratio of the grid was kept between 1.05 and 1.1 in the whole domain and at least twenty cells along every edge of buildings were used (Fig. 10). Three computational grids are generated for each of the geometries, one for every wind direction. In order to avoid convergence problems and maximize numerical accuracy, only hexahedral and prismatic cells were used. Key statistics for each grid are shown in Tables 2 and 3. It can be seen that the *approximated* models are more than 50% more computational expensive than the *simplified* ones, in terms of the number of cells, grid generation and required runtime. Fig. 11 compares the geometry of the actual urban area, the WT model and both CFD models.

As recommended by Blocken (2015), three different blockage ratios

Table 2
Comparison of computational grids (in terms of number of cells) for the *simplified* and *approximated* models.

Wind direction	Simplified model	Approximated model	app/sim
$\alpha = 240°$	13,205,730	23,275,935	1.76
$\alpha = 270°$	11,283,586	20,817,834	1.84
$\alpha = 300°$	11,394,163	19,915,959	1.75

Table 3
Comparison of computational time required for the *simplified* and *approximated* models.

Computational time	Simplified model	Approximated model	app/sim
total time for grid generation (h)	432	687	1.59
total runtime (h)	234	402	1.72

are calculated: the *vertical blockage ratio* BR_H, the *lateral blockage ratio* BR_L and the (*frontal area) blockage ratio BR*. Ideally these ratios should be below 17% for the first two and 3% for the last one. The values given in Eq. (3) below show that this criterion is met for BR_H but not for *BR* and BR_L: especially the value for BR_L is quite high. However, the projected frontal area gives an overly pessimistic estimate of the importance of blockage effects due to the existence of streets in the model through which air can flow. Furthermore, since all measurement positions and all positions of interest are located in the central part of the urban model, the effect of possible artefacts near the edges of the model on observations in these positions is expected to be limited. Regardless, most important for the validation study is that the cross-section of the computational domain matches the WT cross-section, which is the case.

$$BR = \frac{A_{building}}{A_{domain}} = 3.5\% \quad BR_H = \frac{H_{building}}{H_{domain}} = 5.8\% \quad BR_L = \frac{L_{building}}{L_{domain}} = 58.8\% \tag{3}$$

Concerning the other computational settings, the same boundary conditions, inlet conditions, turbulence model, discretization scheme for the equations, algorithm solver and cluster machine are used as in the first step (Section 3).

4.2. Comparison of wind-tunnel and CFD results

4.2.1. Contours of amplification factor

Contours of the amplification factor are analyzed in various horizontal and vertical sections at different heights and widths of the computational domain. Fig. 12 shows the amplification factors $U_{in,0.02m}$, for both CFD models and for three wind directions.

In Fig. 12a–b ($\alpha = 240°$), *Canale Rosciano* is almost aligned with the approach-flow wind direction and, as a result, the wind flow is funneled through the canal. Separation and reversal zones are not observed along the canal for this wind direction. Inside the canal, the wind velocity in the *simplified* model is substantially higher than in the *approximated* one.

In Fig. 12c–d ($\alpha = 270°$), the *Canale Rosciano* is more sheltered from the approaching wind compared to $\alpha = 240°$. The *simplified* model shows higher wind velocities in the central part of the domain (to the North of the *Canale Rosciano*) than the *approximated* one.

In Fig. 12e–f ($\alpha = 300°$), the *Canale Rosciano* is more perpendicular to the approach-flow, and it is therefore to a large degree sheltered by the upstream buildings. The *approximated* model shows higher wind velocities and more extensive leeward zones at the beginning and the end of the canal, respectively. Especially for this wind direction, the CFD simulations are found to be quite sensitive to the geometric detailing. Important differences between the two levels of detail employed in this study are found inside the narrow street and canal, as shown in Fig. 13 for the amplification factor $U_{in,0.6m}$.

Fig. 14 shows contours of the amplification factor $U_{in,0.6m}$ for both CFD models at the centerline of the computational domain for $\alpha = 240°$. Despite the fact that model detail can heavily modify the wind-flow pattern inside the urban district, overall, the thickness of the UBL seems similar in both CFD models. Indeed, Fig. 14 shows almost the same horizontal development of stratification for the *simplified* and *approximated* models, although the maximum height of the buildings is different for both models, i.e. about 0.10 m and 0.15 m (32 and 45 m at full scale) respectively. This is useful information in our understanding of the physical interpretation of displacement height.

4.2.2. Vertical wind profiles

To analyze the streamwise (horizontal) homogeneity of the approach-flow profiles, an empty domain with the same size as that for the urban model (see Section 4.1) is employed. The profiles at the inlet face and at

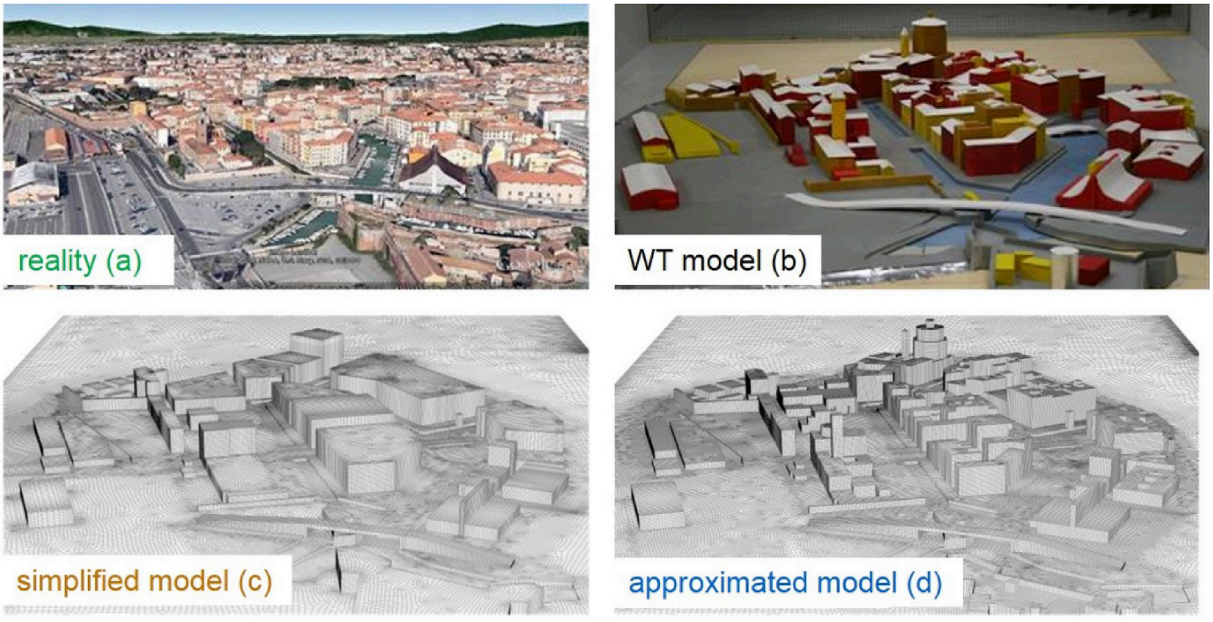

Fig. 11. *Quartiere La Venezia*: view from wind direction $\alpha = 240°$. (a) Photo of the actual urban district, (b) photo of the WT model, (c) computational grid of the *simplified* model, (d) computational grid of the *approximated* model.

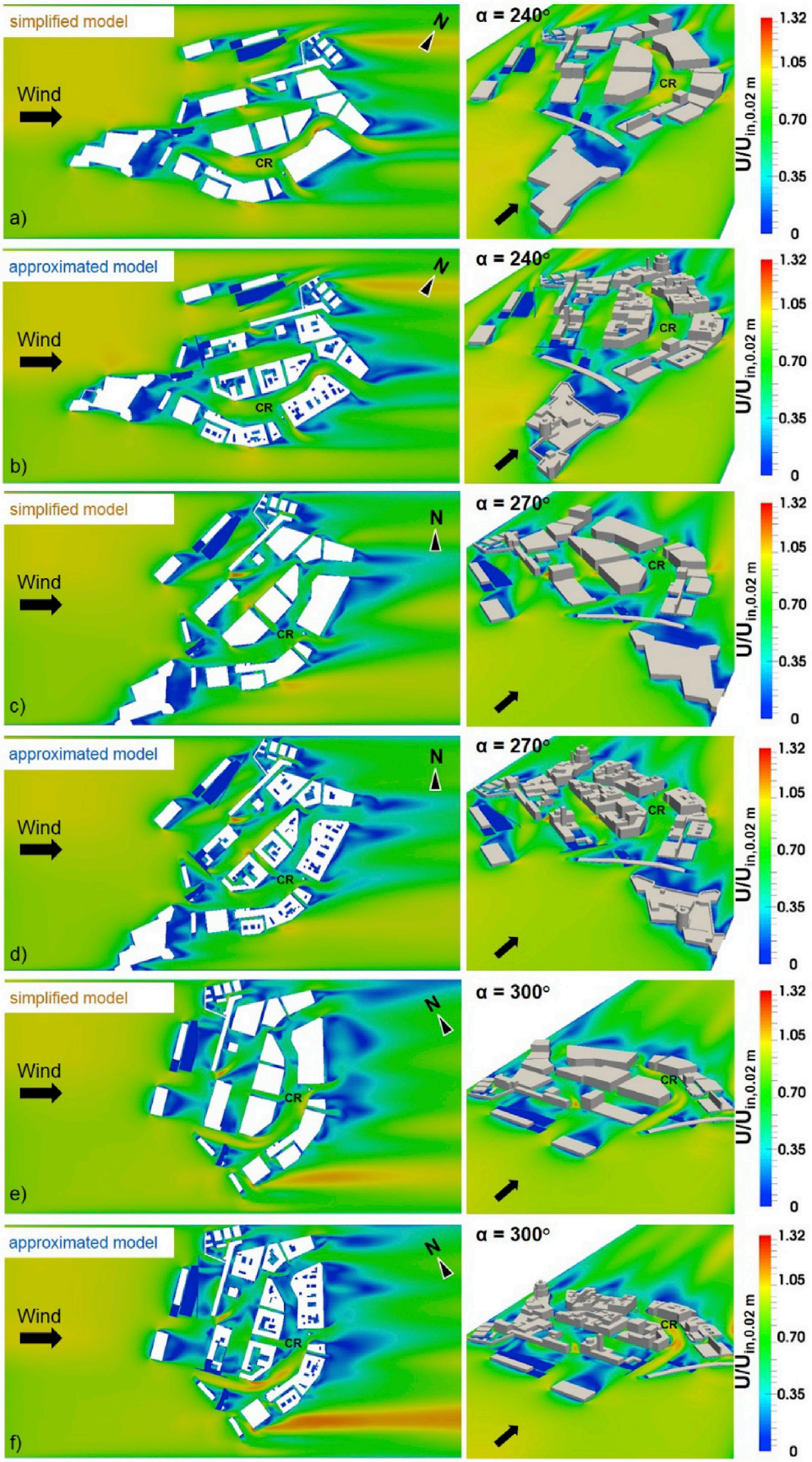

Fig. 12. Contours of amplification factor: comparison between *simplified* and *approximated* geometrical models for wind directions (a, b) $\alpha = 240°$, (c, d) $\alpha = 270°$ and (e, f) $\alpha = 300°$- horizontal sections (left) and axonometric view (right) made at 0.02 m above the bottom (6 m above sea level at full scale). *Canale Rosciano* is indicated by "CR" in the figures.

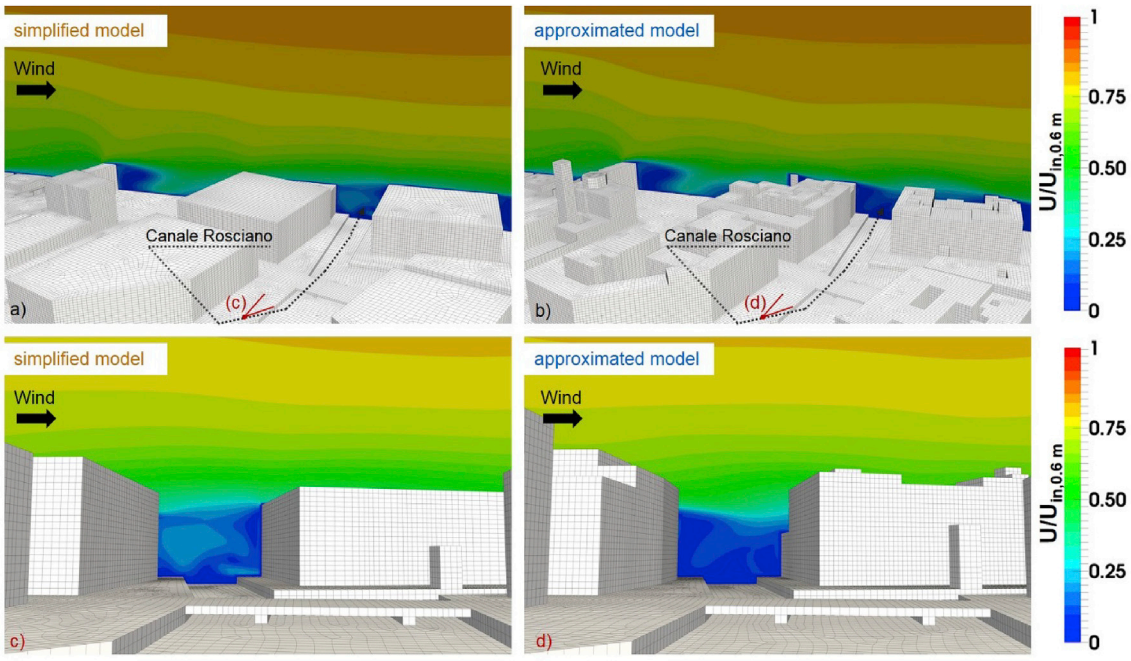

Fig. 13. Contours of amplification factor in vertical centerplane along lines L2 (see Fig. 3a) for the inlet wind direction $\alpha = 300°$: comparison between *simplified* and *approximated* model from (a–b) birdy-eye view, and (c–d) view from *Canale Rosciano*.

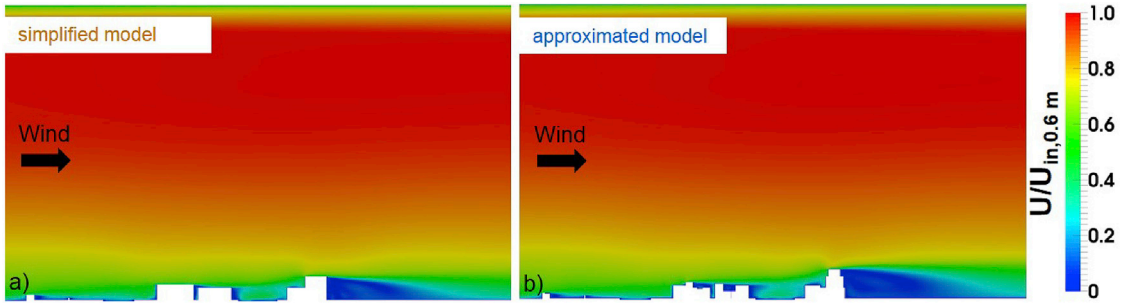

Fig. 14. Contours of amplification factor in vertical centerplane through lines L2 (see Fig. 3a) wind velocity for the inlet wind direction $\alpha = 240°$: comparison between (a) *simplified* and (b) *approximated* models.

the position of the first building of the urban model are compared along the lines L2 (centerline of computational domain) and at 0.02 m above the bottom, yielding a relative difference of only 0.91% (with an increase of the velocity), indicating sufficient horizontal inhomogeneity (Blocken et al., 2007a).

Fig. 15 shows dimensionless mean wind velocity profiles obtained from the WT and CFD models for the three wind directions at four locations. The set of measuring positions placed at the central line of the *Canale Rosciano* ($A2_2$-$A5_2$) were chosen in order to understand the canyoning effects inside the urban district (see Fig. 3b).

Overall, above roughly 0.17 m (50 m full-scale equivalent), corresponding to $z/z_{ref} \cong 0.28$, the mean velocity profiles are fairly undisturbed for all models (WT, *simplified* and *approximated* models) and approximately coincident with the incoming profiles, especially for the wind direction $\alpha = 240°$. For $\alpha = 240°$, the wind is approximately aligned with the entrance of *Canale Rosciano* and can flow between the city blocks rather freely. It is also evident that, when the orientation of the *Canale Rosciano* is more inclined with respect to the incoming wind (from $\alpha = 240°$ to $\alpha = 300°$), at lower heights, the WT and CFD wind velocity profiles are strongly modified by the buildings and the different degrees of precision with which they are represented turn out to have a large effect on the flow, especially inside the narrow street and canal.

Fig. 15a ($\alpha = 240°$): at position $A2_2$, where the incoming flow is aligned with the canal, the agreement between CFD and WT results is quite satisfactory. At position $A3_2$ the CFD model predictions are less accurate. Intentionally chosen, this position is located directly leeward of the important bridge near the city center and in the middle of a crossroads. At position $A4_2$ the level of detail of the CFD model plays a key role. In this part of the canal the incoming flow is no longer perfectly aligned with it, and the wake effects due to the presence of the buildings can be extremely dependent on their shape. Whereas the mean velocity profile of the *approximated* model shows a very similar trend compared with the WT profile, the *simplified* model displays a larger gap to the WT results between 0.11 and 0.28 of z/z_{ref}. In the last position $A5_2$, which is located in the middle of a canal curve, the *approximated* model again leads to a better prediction than the *simplified* one. Overall, for this wind direction, the *approximated* model shows better agreement with WT results than the *simplified* one. This also holds true for the measuring positions that are not reported here.

Fig. 15b ($\alpha = 270°$): at position $A2_2$ the agreement between the CFD models and the WT results is very close in the higher part of the domain down to $z/z_{ref} = 0.1$ (18 m full scale). However, the discrepancy between WT and CFD results is substantial close to the ground. At positions $A3_2$ and $A4_2$ important differences are found between 0 and 0.2 z/z_{ref}. As previously stated, these positions are located directly leeward of some buildings (see also Fig. 12c–d), where the results are affected by the

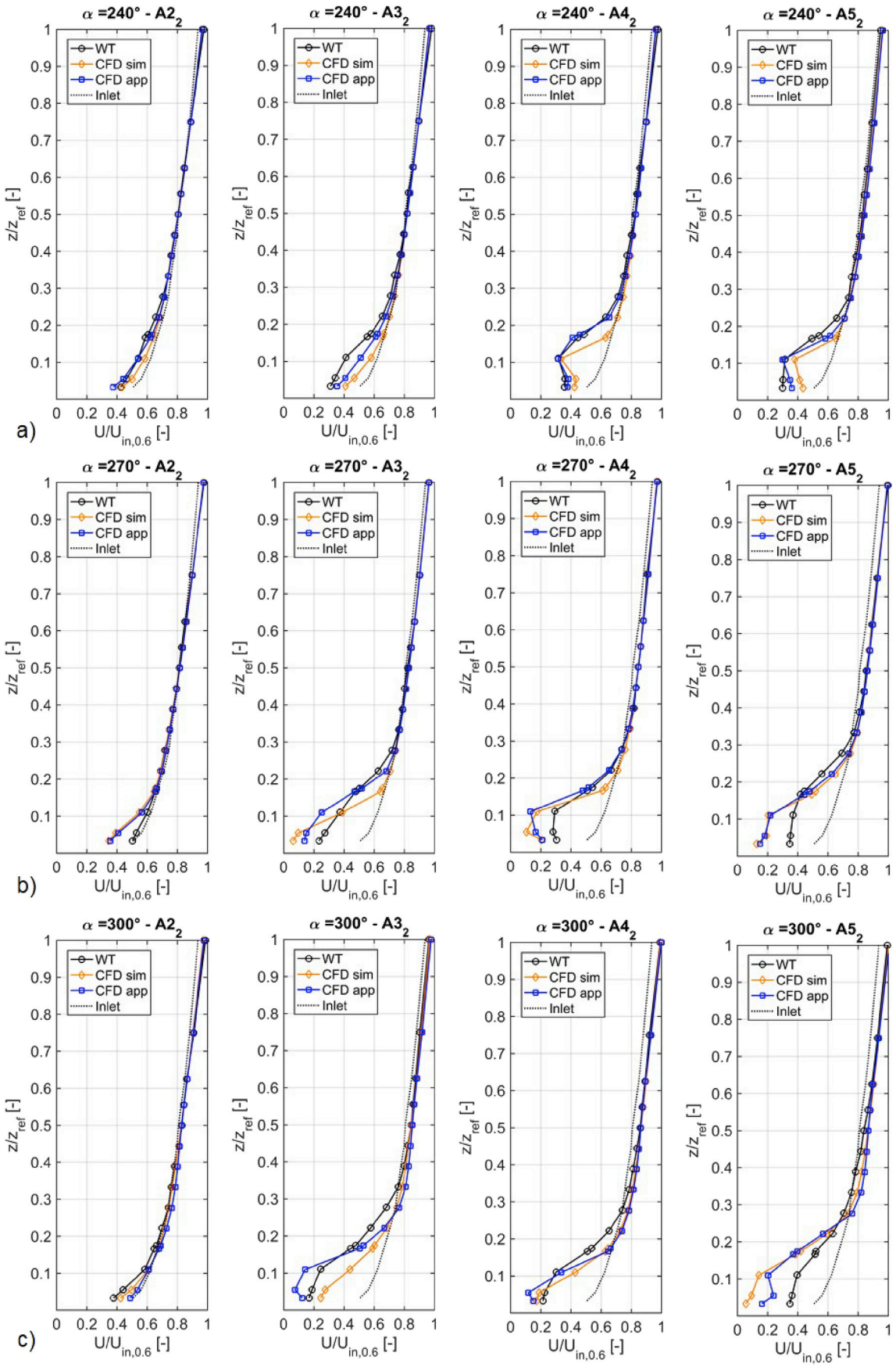

Fig. 15. Comparison of the vertical mean wind velocity profiles ($z_{ref} = 0.60$ m) along the lines $A2_2$-$A5_2$ for the inlet directions (a) $\alpha = 240°$, (b) $\alpha = 270°$ and (c) $\alpha = 300°$, for the *simplified* model (CFD sim), *approximated* model (CFD app), and WT model (WT). The inlet profile (black dashed line) is also shown for comparison.

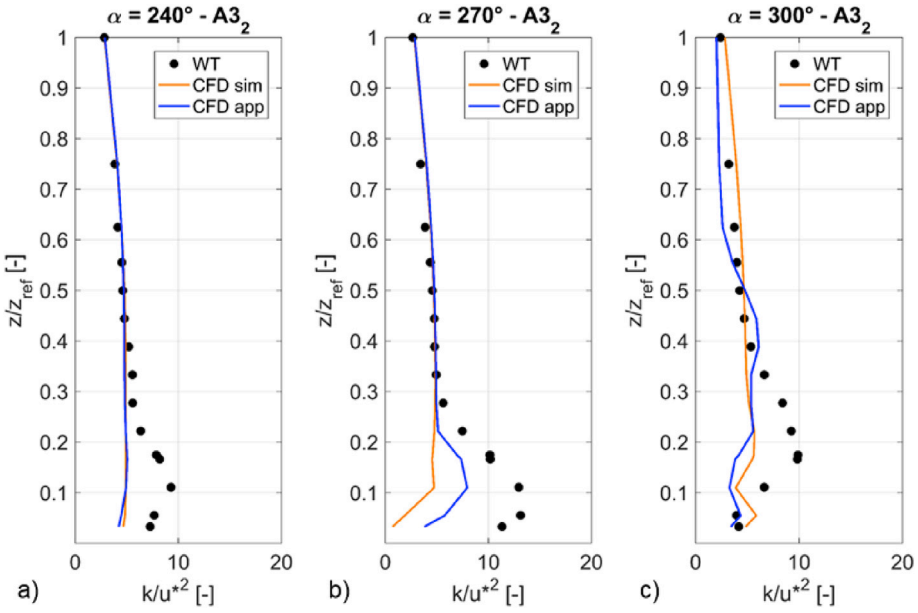

Fig. 16. Comparison of turbulent kinetic energy profiles (z_{ref} = 0.60 m) along the line $A3_2$ for the inlet directions (a) $\alpha = 240°$, (b) $\alpha = 270°$, (c) $\alpha = 300°$ using the *simplified* model (CFD sim), *approximated* model (CFD app), and WT model (WT).

underestimation of the turbulent kinetic energy k due to the steady-state RANS approach here adopted. As an example, Fig. 16 shows the underestimation of the turbulent kinetic energy for all wind directions at position $A3_2$. The quantitative agreement between WT and CFD results is unsatisfactory for this wind direction, although the qualitative wind profile development of the models inside the *Canale Rosciano* (from position $A2_2$ to $A5_2$) is somewhat similar. This was probably due to the canyoning effects along the water canal. The worst agreement between the WT and CFD results occurs at position $A2_2$ below $z/z_{ref} = 0.15$, and at positions $A3_2$, $A4_2$ and $A5_2$ below $z/z_{ref} = 0.30$.

Fig. 15c ($\alpha = 300°$): the worst performance of the CFD models is obtained for this wind direction. The buildings located at the edge of the *Canale Rosciano* represent a barrier for the wind flow. Only for position $A2_2$, located windward of the canal, the comparison is satisfactory. For the rest of the positions ($A3_2$, $A4_2$ and $A5_2$) the CFD profiles are quite different from the WT ones. The wind flow is not channeled along the *Canale Rosciano* and canyoning effects occur in the simulations behind the buildings placed at the edge of the channel (see Fig. 12e–f). This aspect explains the trend of the profiles at different positions. The worst agreement between the WT and CFD results is observed at position $A2_2$ below $z/z_{ref} = 0.1$, and at positions $A3_2$, $A4_2$ and $A5_2$ below $z/z_{ref} = 0.40$.

Finally, in order to understand the different wind flow patterns produced by two CFD models (i.e. *simplified* and *approximated* models) in the downstream part of the computational domain, mean velocity profiles of two CFD models are compared at the 27 positions ($L1_{6\text{-}14}$, $L2_{6\text{-}14}$, $L3_{6\text{-}14}$) already shown in Fig. 3a. The mean velocity profiles monitored along the centerline of the computational domain (from $L2_6$ to $L2_{14}$) and for the three wind directions considered, are graphically displayed in Fig. 17. The axes show the ratio $U/U_{in,0,6m}$ (abscissa) vs. normalized reference height z/z_{ref} (ordinate), with the incoming wind velocity $U_{in,0,6m}$ measured at a reference height of $z_{ref} = 0.6$ m as normalization factor.

Overall, the two CFD models show, for each wind direction, a different wind velocity profile development in the downstream part of the computational domain, from the last building of the urban district (at about the position $L2_5$ and $L2_6$) to the outlet face (Fig. 17). It is worth to note that, for the *simplified* model, where the tallest building (about 0.10 m) is lower than the equivalent of the *approximated* model (about 0.15 m), the wind velocity profile reaches almost a complete equilibrium condition, i.e. it does not change anymore, in the downwind distance (from the position $L2_6$ to the outlet face of the domain). In contrast, for the *approximated* model, for which the mismatch of roughness heights is larger than the *simplified* model, the mean velocity profile needs a larger downwind distance to reach an equilibrium condition.

4.2.3. Error analysis along vertical lines

A comparison between the CFD and WT test results is made along vertical lines at the positions $A2_1$ and $A4_1$ (see also Fig. 3b) for 15 heights and three wind directions. Normalized mean wind velocities in the CFD results and WT data are plotted against each other in Fig. 18. The abscissa reports the ratio between the mean wind velocity measured at height z and the reference mean wind velocity measured at $z = 0.6$ m (U_{ref}) in the WT tests; the ordinate axis shows the same ratio for the CFD results. Fig. 18a shows better agreement between the *approximated* model and the WT model than between the *simplified* and the WT model. In the latter case the velocity ratio is substantially overestimated compared to the WT data. In contrast, the *approximated* model shows some underestimation of the velocity values close to the ground. For the inlet wind direction $\alpha = 270°$, shown in Fig. 18b, discrepancies are observed between the CFD and WT velocity ratios, especially at position $A4_1$ near the ground. This is found for both CFD models, probably due to the flow reversal zones close to the walls (see Fig. 12c–d). The results shown in Fig. 18c are consistent with those for the central line of the *Canale Rosciano* (Fig. 15c). The large deviations between CFD and WT results highlighted at position $A2_1$ for this inflow direction ($\alpha = 300°$) can be due to the zone of flow separation present at the entrance of the canal (see Fig. 12e–f). Underestimation and overestimation of the velocity ratios occurs at position $A4_1$, in the lower and higher part of the profiles, respectively. Fig. 18 clearly shows one of the limitations of this study. As a matter of fact, the accuracy that can be achieved is most likely limited by the deficiencies of the 3D steady state RANS approach. The use of a more accurate geometry may therefore not lead to improved predictions within the areas where non-stationary wind-flow patterns occur. This limitation was already pointed out, for instance, by Murakami (1993), Tominaga et al. (2008b) and Blocken et al. (2016), who discussed this issue for building aerodynamics and by Burlando et al. (2015b), who discussed this issue using an analogous CFD model to simulate the flow around a vertical axis wind turbine.

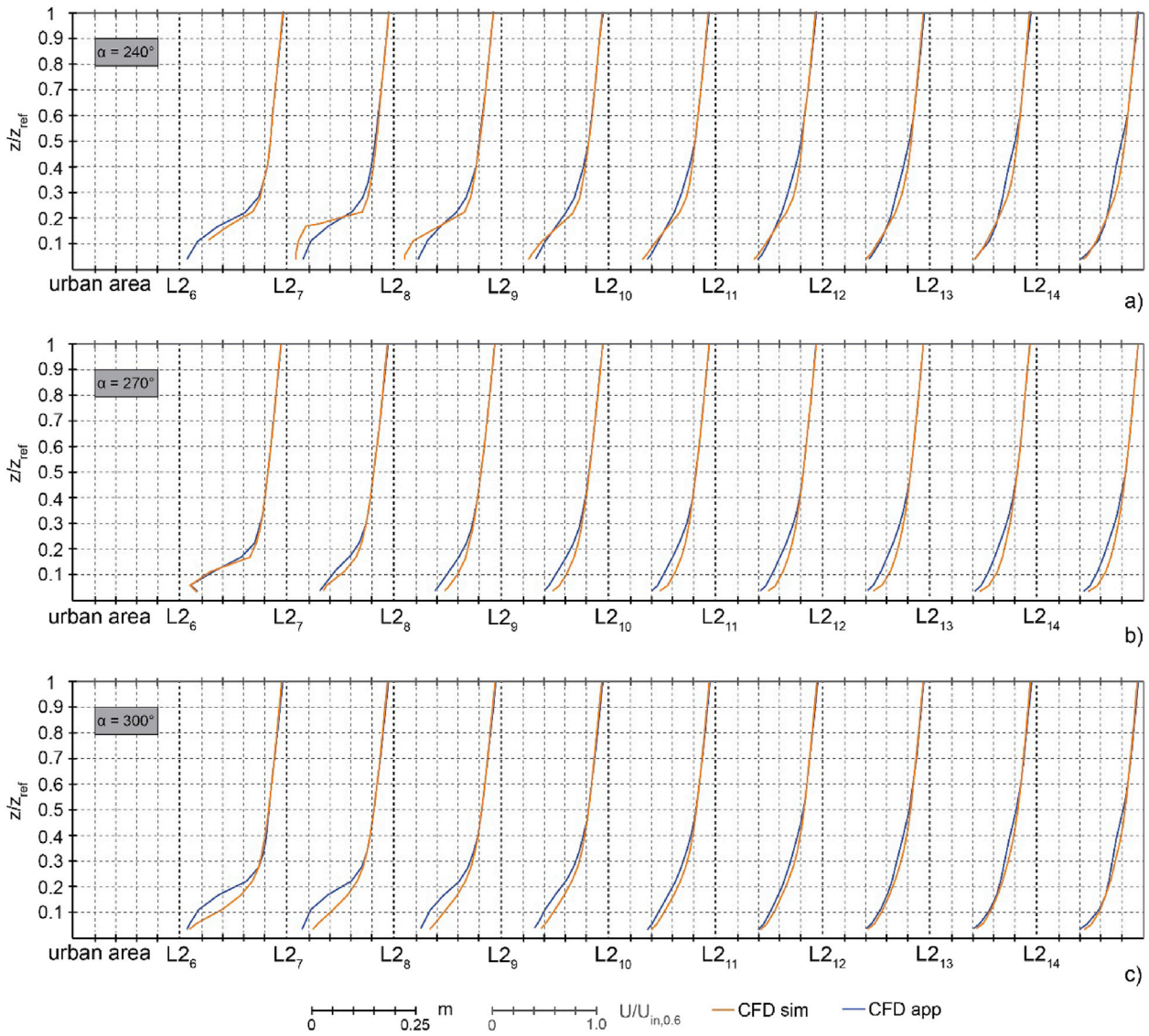

Fig. 17. Comparison of the vertical mean wind velocity profiles along the lines $L2_6$ - $L2_{14}$ and for the inlet directions (a) $\alpha = 240°$, (b) $\alpha = 270°$ and (c) $\alpha = 300°$, for the *simplified* model (CFD sim) and *approximated* model (CFD app).

5. Deviations caused by geometrical simplifications

5.1. Validation metrics

The statistical performance of both CFD models is evaluated (Chang and Hanna, 2004; Gousseau et al., 2013) in order to quantify the agreement in the mean velocity U between CFD and WT results. Based on the study by Schatzmann et al. (2010), four different validation metrics are used:

$$\text{Fractional Bias (FB)} \quad (FB) = 2\frac{\left(\overline{U_{WT}} - \overline{U_{CFD}}\right)}{\overline{U_{WT}} + \overline{U_{CFD}}} \tag{4}$$

$$\text{Normalized Mean Square Error } (NMSE) \quad NMSE = \frac{\overline{(U_{WT} - U_{CFD})}^2}{\overline{U_{WT}} \cdot \overline{U_{CFD}}} \tag{5}$$

$$\text{Correlation coefficient } (R) \quad R = \frac{\left(\overline{U_{WT} - \overline{U_{WT}}}\right)\overline{\left(U_{CFD} - \overline{U_{CFD}}\right)}}{\sigma_{U_{WT}} \cdot \sigma_{U_{CFD}}} \tag{6}$$

$$\text{Fraction of data points } (FAC1.3) \text{ that satisfy: } \quad 1/1.3 \approx 0.77 \leq \frac{U_{CFD}}{U_{WT}} \leq 1.3 \tag{7}$$

here $\overline{U_{WT}}$ is the mean wind velocity magnitude (m/s) from the WT experiments, $\overline{U_{CFD}}$ is the mean wind velocity magnitude from the CFD simulations (m/s) using the *simplified* or *approximated* model, and σ is the standard deviation over a specific dataset. The ideal values corresponding to complete agreement between CFD and WT are $FB = 0$, $NMSE = 0$, $R = 1$ and $FAC1.3 = 1$.

5.2. Statistical performance: wind velocities in horizontal planes

The validation metrics were calculated in horizontal planes at 15 heights (z) from 0.02 m to 0.6 m above the bottom (corresponding to 6 and 180 m above sea level at full scale) for all measuring positions A and L (overall 25 points) and for all inlet wind directions ($\alpha = 240°$, $\alpha = 270°$ and $\alpha = 300°$). Results for $z = 0.02$ m above the bottom are given in Table 4 for each considered wind direction. The results of Table 4 are based on data which are graphically displayed in Fig. 19. On the abscissa, the mean wind velocity value U_{WT} measured at all available positions is

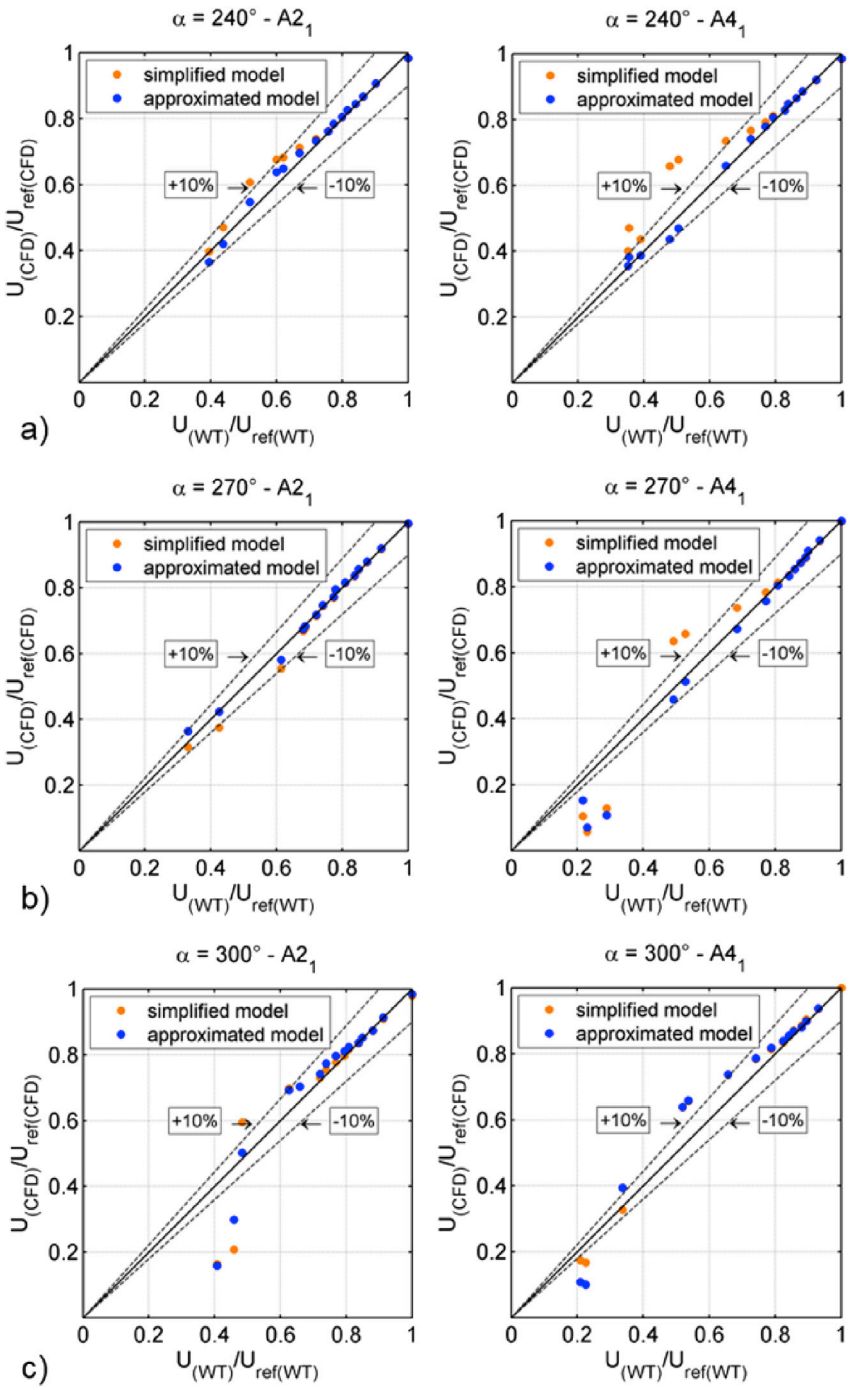

Fig. 18. Comparison of normalized mean wind velocity values along the vertical profiles $A2_1$ and $A4_1$ for inlet directions (a) $\alpha = 240°$, (b) $\alpha = 270°$ and (c) $\alpha = 300°$ for the WT model (WT), *simplified* and *approximated* models. Dashed lines correspond to 10% errors.

displayed, normalized with respect to the mean inlet wind velocity magnitude taken at reference height $U_{in,0.02}$ (6 m above sea level at full scale). The equivalent ratio $U_{CFD}/U_{in,0.02}$ of the WT data is reported on the ordinate.

For a wind direction of $\alpha = 240°$ the *FB* values of the *approximated* model clearly shows a tighter distribution around the diagonal compared to the *simplified* model, indicating better agreement. For $\alpha = 270°$ the same *FB* value is obtained for both CFD models while for $\alpha = 300°$ the *simplified* model performed better than the *approximated* one. A similar trend is observed for the *NMSE* which shows better performance of the *approximated* model for $\alpha = 240°$. Its performance becomes comparable to that of the *simplified* model for $\alpha = 270°$ while it is outperformed by the *simplified* model for $\alpha = 300°$. The *R* of the *approximated* models is in general quite satisfactory. For $\alpha = 240°$ and $\alpha = 300°$ the *approximated* model clearly performed better than the *simplified* model while they showed similar performance for $\alpha = 270°$. Finally, the metric *FAC1.3* is used to understand how many data positions fall within 30% of WT data. No difference in the performance of both CFD models is observed in this metric for $\alpha = 270°$ and $\alpha = 300°$, while the *approximated* model performed much better for $\alpha = 240°$.

5.3. Influence of geometrical simplifications on the total drag

In order to assess the effect of the geometrical simplifications on the total drag (*D*), this parameter was calculated for both the *simplified* and *approximated* models (D_{sim} and D_{app}) and for the three wind directions

Table 4
Validation metrics (*FB* = Fractional Bias, *NMSE* = Normalized Mean Square Error, *R* = correlation coefficient, *FAC1.3* = Fraction of data within a factor of 1.3) for both CFD models, three inlet wind directions ($\alpha = 240°$, $\alpha = 270°$, $\alpha = 300°$), and 25 measurement positions (A and L) at $z = 0.02$ m above the bottom, corresponding to 6 m above the sea level at full scale. Also indicated are the number of samples (measurement positions) that are not occupied by the urban model and are therefore available for statistical analysis (note that this depends on the wind direction as positions L are fixed with respect to the WT section).

($\alpha = 240°$) for z = 0.02 m	CFD sim *vs* WT	CFD app *vs* WT	ideal value
FB	−0.15	−0.04	0
NMSE	0.07	0.04	0
R	0.64	0.77	1
FAC1.3	0.67	0.89	1
samples	18 of 25	18 of 25	25
($\alpha = 270°$) for z = 0.02 m	CFD sim *vs* WT	CFD app *vs* WT	ideal value
FB	0.23	0.23	0
NMSE	0.13	0.12	0
R	0.75	0.76	1
FAC1.3	0.50	0.50	1
samples	20 of 25	20 of 25	25
($\alpha = 300°$) for z = 0.02 m	CFD sim *vs* WT	CFD app *vs* WT	ideal value
FB	0.25	0.30	0
NMSE	0.32	0.34	0
R	0.35	0.53	1
FAC1.3	0.41	0.41	1
samples	17 of 25	17 of 25	25

considered. As expected, for all the CFD cases the most significant contribution to the total drag is given by the pressure drag associated to the bluff bodies (i.e. buildings and bridges), whereas the viscous drag contribution is confined between 2% and 6%, depending on the CFD case considered. In Table 5 the ratio between D and $D_{sim,\ 270°}$ (chosen as reference value) is shown for all the CFD models. For all the wind directions considered, the drag for the *approximated* model is higher than the *simplified* one, i.e. +20.2% for $\alpha = 240°$, +19.0% for $\alpha = 270°$ and +8.1% for $\alpha = 300°$, as reported in the last row of Table 5, where the relative difference between two CFD models is calculated as $((D_{app}/D_{sim,270°})-(D_{sim}/D_{sim,270°})/(D_{sim}/D_{sim,270°}))$. This is possibly attributable to the higher mean height of the buildings, which yields a higher contribution of the pressure drag as well. In addition, the total drag also changes according to the wind direction considered.

6. Discussion and limitations

In this case study, the 3D steady-state RANS approach with the *realizable k-ε* turbulence model was applied to simulate mean wind-velocity patterns in a single block of *Quartiere La Venezia* and in the whole urban district reproduced at reduced scale (1:300). A portion of the WT section was reproduced by the computational domain in order to facilitate the comparison between WT and CFD results. This study is based on several assumptions:

- The study was performed for only a single city district. Nevertheless, the selected area may be considered representative of many historic towns including different types of buildings and narrow and curved streets.
- WT tests and CFD simulations were performed only for a neutrally stratified ABL flow, which typically occurs at the highest wind velocities.
- Three geometries with different degrees of precision were analyzed only for a single block of *Quartiere La Venezia*, since the *detailed* model of the whole urban district was found to be extremely computational demanding.
- The method used to estimate the height of the buildings (the average between the heights of the peak and eaves of roofs) of the *approximated* model may be not completely representative of buildings with roofs particularly slanted.
- The CFD simulations were performed using the 3D steady-state RANS approach, which is known to be deficient especially in separation zones. Large-Eddy Simulation (LES) are currently planned in order to investigate the impact of this limitation.
- Only a limited number of measuring positions (25 positions in the horizontal plane) was taken into account during the WT tests and subsequently used to validate the CFD results. For each point, however, 15 different heights were monitored, so that the overall number of points is actually equal to 375. These points, in turn, were measured for three wind directions, which means 1125 independent measurements.

In spite of these limitations, the CFD simulations of the urban district showed a satisfactory agreement with the WT tests for wind direction $\alpha = 240°$ when the finer geometry (*approximated* model) was used.

7. Summary and conclusions

In this paper the local-scale forcing effects on wind flows in an urban environment were evaluated. In the first step, 3D steady-state RANS simulations were performed on a single block of a selected case study -

Table 5
Comparison of total drag force between *simplified* and *approximated* models. The total drag values are non-dimensionalized with respect to the total drag force of *simplified* model found for the wind direction $\alpha = 270°$. The ratio in terms of relative difference between two CFD models is also reported in the last row of the table.

Total drag ratio	$\alpha = 240°$	$\alpha = 270°$	$\alpha = 300°$
$D_{sim}/D_{sim,270°}$	0.84	1.00	1.11
$D_{app}/D_{sim,270°}$	1.01	1.19	1.20
Diff. (%)	20.2%	19.0%	8.1%

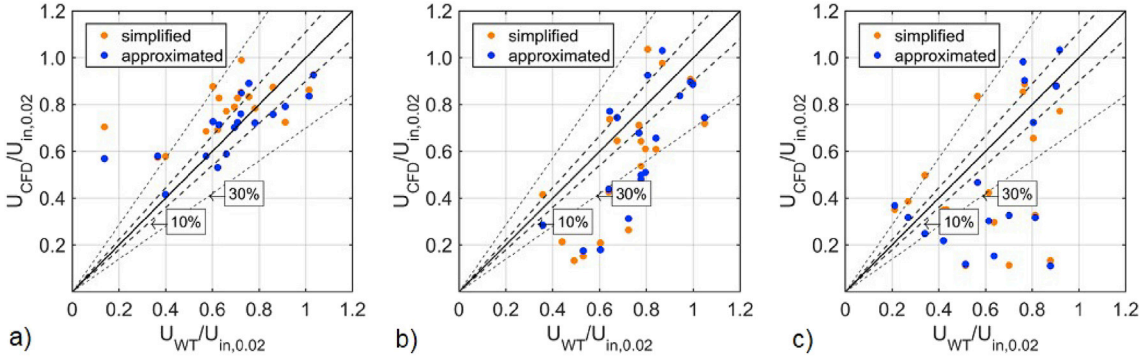

Fig. 19. Comparison of CFD and WT data at the monitored positions (A and L) for inlet directions: (a) $\alpha = 240°$, (b) $\alpha = 270°$, (c) $\alpha = 300°$ at a height $z = 0.02$ m above the bottom (corresponding to 6 m above sea level at full scale). Dashed black lines correspond to 10% and 30% of errors.

Quartiere la Venezia in Livorno city (Italy) - for one wind direction ($\alpha = 240°$) and three geometries with different degrees of precision, i.e. *simplified*, *approximated* and *detailed* models. Based on the numerical results found in the first step, a *simplified* and *approximated* model of the urban district *Quartiere La Venezia* were generated and simulated in the second step, using the same computational settings employed in the first step (dimension of domain, boundary conditions, turbulence model, discretization schemes for the equations, algorithm solver). In order to investigate to which extent geometrical model details can affect the CFD results, the mean wind velocity profiles of both CFD models at 25 positions for 15 heights each and three different wind directions were compared with the WT results. In order to quantify the agreement between the WT and the CFD results, the statistical performance was evaluated using four different validation metrics: *FB*, *NMSE*, *R* and *FAC1.3*.

From the first step of this study, the following observations can be made:

- The *simplified* model showed large difference in terms of mean velocity with respect to the *approximated* and *detailed* models, mostly in the lower part of the wind velocity profiles (Section 3.4).
- The *approximated* and *detailed* models showed a satisfactory agreement both upstream and downstream of the single block (Section 3.4). The small differences in terms of mean velocity found mostly in the courtyard of the buildings, between two CFD models, do not justify probably a very high computational effort required to realize and simulate an eventual detailed model of the entire urban district (Section 3.4).

From the second step of this study, the following observations can be made:

- The mean velocity contours showed the sensitivity of the simulations to the different degrees of model precision. The largest differences between the flow fields in the *approximated* and *simplified* models were found in the narrow streets and canal, especially for the wind direction $\alpha = 240°$ (Section 4.2.1).
- Although the geometric detail can affect the wind-flow pattern inside the urban district, the thickness of the UBL was similar for both CFD models (Section 4.2.1).
- For the wind directions $\alpha = 270°$ and $\alpha = 300°$, corresponding to a decrease of the flow alignment with respect to the entrance of *Canale Rosciano*, the agreement between CFD and WT results decreased (Section 4.2.2).
- The CFD results showed an unsatisfactory correspondence between the CFD and WT results in locations where non-stationary phenomena occurred. It is likely that here the 3D steady-state RANS approach becomes the main source of error, in which case a more detailed geometry will not improve the flow prediction.
- The validation metrics (*FB*, *NMSE*, *R* and *FAC1.3*) confirmed that the finer geometry (*approximated* model) on average assures notably better performance than the coarse one (*simplified* model) (Section 5.2).
- The geometrical simplifications applied to the urban model of *Quartiere La Venezia* affected the results also in terms of total drag. The *approximated* model resulted in a higher total drag with respect to the *simplified* model for all wind directions considered (Section 5.3).

Overall, wind flow modeling in urban areas is affected by many errors and uncertainties related to the inlet conditions, boundary conditions, numerical approach (RANS, LES, DNS), turbulence models, etc. A discussion of all these errors and uncertainties is beyond the scope of the present paper, but the future intention is to quantify their relative importance for the urban area investigated in this paper. In particular, numerical investigations on the same urban model (at scale 1:300) are in progress to quantify the uncertainties concerning inlet conditions as well as the numerical approach (RANS, LES, …).

Acknowledgements

The authors gratefully acknowledge the Port Authority of Livorno for the data of its anemometric monitoring network. All the monitoring devices and the HPC system at DICCA have been funded by the European Cross-border Programme Italy/France *"Maritime"* 2007–2013 through the "Wind and Port" (CUP: B87E09000000007) and "Wind, Ports, and Sea" (CUP: B82F13000100005) projects.

This research has been carried out in the framework of the Project "Wind monitoring, simulation and forecasting for the smart management and safety of port, urban and territorial systems" funded by "Compagnia di San Paolo" (ID ROL: 9820) in the period 2016–2018.

References

AIAA, 1998. Guide for the Verification and validation of computational fluid dynamics simulations. AIAA. G-077–1998, ISBN: 1563472856.
An, K., Fung, J.C.H., Yim, S.H.L., 2013. Sensitivity of inflow boundary conditions on downstream wind and turbulence profiles through building obstacles using a CFD approach. J. Wind Eng. Ind. Aerodyn. 115, 137–149.
Architectural Institute of Japan, 2004. Recommendations for Loads on Buildings. Architectural Institute of Japan (in Japanese).
Baker, C.J., 2007. Wind engineering – past, present and future. J. Wind Eng. Ind. Aerodyn. 95, 843–870.
Barlow, J.F., 2013. The wind that shakes the buildings: wind engineering from a boundary layer meteorology perspective. In: Owen, J.S., et al. (Eds.), Fifty Years of Wind Engineering: Prestige Lectures from the Sixth European and African Conference on Wind Engineering. University of Birmingham.
Blocken, B., 2015. Computational Fluid Dynamics for Urban Physics: importance, scales, possibilities, limitations and ten tips and tricks towards accurate and reliable simulations. Build. Environ. 91, 219–245.
Blocken, B., 2014. 50 years of computational wind engineering: past, present and future. J. Wind Eng. Ind. Aerodyn. 129, 69–102.
Blocken, B., Janssen, W.D., van Hooff, T., 2012. CFD simulation for pedestrian wind comfort and wind safety in urban areas: general decision framework and case study for the Eindhoven University campus. Environ. Model. Softw. 30, 15–34.
Blocken, B., Stathopoulos, T., Carmeliet, J., 2007a. CFD simulation of the atmospheric boundary layer: wall function problems. Atmos. Environ. 41, 238–252.
Blocken, B., Carmeliet, J., Stathopoulos, T., 2007b. CFD evaluation of the wind speed conditions in passages between buildings – effect of wall-function roughness modifications on the atmospheric boundary layer flow. J. Wind Eng. Ind. Aerodyn. 95, 941–962.
Blocken, B., Stathopoulos, T., van Beeck, J.P.A.J., 2016. Pedestrian-level wind conditions around buildings: review of wind-tunnel and CFD techniques and their accuracy for wind comfort assessment. Build. Environ. 100, 50–81.
Bossard, M., Feranec, J., Otahel, J., 2000. Corine Land Cover Technical Guide-addendum 2000. Technical Report No 40. EFA, Copenhagen.
Britter, R.E., Hanna, S.R., 2003. Flow and dispersion in urban areas. Annu. Rev. Fluid Mech. 35, 469–496.
Burlando, M., De Gaetano, P., Pizzo, M., Repetto, M.P., Solari, G., Tizzi, M., Bonino, G., 2015a. The European project wind, ports, and sea. In: Proceedings of the 14th International Conference on Wind Engineering, Porto Alegre, Brazil, June 21–26.
Burlando, M., Ricci, A., Freda, A., Repetto, M.P., 2015b. Numerical and experimental methods to investigate the behaviour of vertical-axis wind turbines with stators. J. Wind Eng. Ind. Aerodyn. 144, 125–133.
Carpentieri, M., Robins, A.G., 2015. Influence of urban morphology on air flow over building arrays. J. Wind Eng. Ind. Aerodyn. 145, 61–74.
Casey, M., Wintergerste, T., 2000. Best Practice Guidelines, ERCOFTAC Special Interest Group on Quality and Trust in Industrial CFD. ERCOFTAC, Brussels.
Chang, J.C., Hanna, S.R., 2004. Air quality model performance evaluation. Meteorol. Atmos. Phys. 87, 167–196.
Cebeci, T., Bradshaw, P., 1977. Momentum Transfer in Boundary Layers. Hemisphere Publishing Corporation, New York.
Chang, C.H., Meroney, R.N., 2003. Concentration and flow distributions in urban street canyons: wind tunnel and computational data. J. Wind Eng. Ind. Aerodyn. 91, 1141–1154.
Cheng, W.C., Porté-Agel, F., 2015. Adjustment of turbulent boundary-layer flow to idealized urban surfaces: a large-eddy simulation study. Bound. - Layer. Meteorol. 129, 1–23.
Coceal, O., Belcher, S.E., 2004. A canopy model of mean winds through urban areas. Q. J. R. Meteorol. Soc. 130, 1349–1372.
Emory, M., Larsson, J., Iaccarino, G., 2013. Modeling of structural uncertainties in Reynolds-averaged Navier-Stokes closures. Phys. Fluids 25, 110822.
Fernando, H.J.S., 2010. Fluid dynamics of urban atmospheres in complex terrain. Annu. Rev. fluid Mech. 42, 365–389.
Fernando, H.J.S., Zajiic, D., Di Sabatino, S., Dimitrova, R., Hedquist, B., Dallman, A., 2010. Flow, turbulence and pollutant dispersion in urban atmospheres. Phys. Fluids 22, 051301–1–20.
Ferziger, J.H., Perić, M., 2002. Computational Methods for Fluid Dynamics, third ed. Springer-Verlag, ISBN 3-540-42074-6.
Franke, J., Hellsten, A., Schlünzen, H., Carissimo, B., 2007. COST Action 732 Quality Assurance and Improvement of Microscale Meteorological Models.

Franke, J., 2006. Recommendations of the COST action C14 on the use of CFD in predicting pedestrian wind environment. In: The Fourth International Symposium on Computational Wind Engineering, Yokohama, Japan, July 2006.
García Sánchez, C., Philips, D.A., Gorlé, C., 2014. Quantifying inflow uncertainties for CFD simulations of the flow in downtown Oklahoma City. Build. Environ. 78, 118–129.
Gorlé, C., Garcia-Sanchez, C., Iaccarino, G., 2015. Quantifying inflow and RANS turbulence model form uncertainties for wind engineering flows. J. Wind Eng. Ind. Aerodyn. 144, 202–212.
Gousseau, P., Blocken, B., van Heijst, G.J.F., 2013. Quality assessment of Large-Eddy Simulations of wind flow around a high-rise building: validation and solution verification. Comput. Fluids 79, 120–133.
Hargreaves, D.M., Wright, N.G., 2007. On the use of the k–ε model in commercial CFD software to model the neutral atmospheric boundary layer. J. Wind Eng. Ind. Aerodyn. 95 (5), 355–369.
Hertwig, D., Efthimiou, G.C., Bartzis, J.G., Leitl, B., 2012. CFD-RANS model validation of turbulent flow in a semi-idealized urban canopy. J. Wind Eng. Ind. Aerodyn. 111, 61–72.
Janssen, W.D., Blocken, B., van Hooff, T., 2013. Pedestrian wind comfort around buildings: comparison of wind comfort criteria based on whole-flow field data for a complex case study. Build. Environ. 59, 547–562.
Launder, B.E., Spalding, D.B., 1974. The numerical computation of turbulent flows. Comput. Methods Appl. Mech. Eng. 3, 269–289.
Meroney, R.N., 2016. Ten questions concerning hybrid computational/physical model simulation of wind flow in the built environment. Build. Environ. 96, 12–21.
Montazeri, H., Blocken, B., Janssen, W.D., van Hooff, T., 2013. CFD evaluation of new second-skin facade concept for wind comfort on building balconies: case-study for the Park Tower in Antwerp. Build. Environ. 68, 179–192.
Murakami, S., 1993. Comparison of various turbulence models applied to a bluff body. J. Wind Eng. Ind. Aerodyn. 46–47, 21–36.
Murakami, S., 1990. Computational wind engineering. J. Wind Eng. Ind. Aerodyn. 36, 517–538.
Oberkampf, W.L., Trucano, T.G., Hirsch, C., 2004. Verification, validation, and predictive capability in computational engineering and physics. Appl. Mech. Rev. 57, 345–384.
Patankar, S.V., 1980. Numerical Heat Transfer and Fluid Flow. McGraw-Hill book company, ISBN 0-07-048740-5.
Razak, A.A., Hagishima, A., Ikegaya, N., Tanimoto, J., 2013. Analysis of airflow over building arrays for assessment of urban wind environment. Build. Environ. 59, 56–65.
Repetto, M.P., Burlando, M., Solari, G., De Gaetano, P., Pizzo, M., Tizzi, M., 2017. A web-based GIS platform for the safe management and risk assessment of complex structural and infrastructural systems exposed to wind. Adv. Eng. Softw. http://dx.doi.org/10.1016/j.advengsoft.2017.03.002 (in press).
Ricci, A., Burlando, M., Freda, A., Repetto, M.P., 2017. Wind tunnel measurements of the urban boundary layer development over a historical district in Italy. Build. Environ. 111, 192–206.
Schatzmann, M., Olesen, H., Franke, J., 2010. COST 732 model evaluation case studies: approach and results. COST Action 732.
Shih, T.H., Liou, W.W., Shabbir, A., Zhu, J., 1995. A new k-ε eddy-viscosity model for high Reynolds number turbulent flows e model development and validation. Comput. Fluids 24, 227–238.
Solari, G., Repetto, M.P., Burlando, M., De Gaetano, P., Parodi, M., Pizzo, M., Tizzi, M., 2012. The wind forecast for safety management of port areas. J. Wind Eng. Ind. Aerodyn. 104–106, 266–277.
Stathopoulos, T., 1997. Computational wind engineering: past achievements and future challenges. J. Wind Eng. Ind. Aerodyn. 67–68, 509–532.
Tominaga, Y., Mochida, A., Yoshie, R., Kataoka, H., Nozu, T., Yoshikawa, M., et al., 2008a. AIJ guidelines for practical applications of CFD to pedestrian wind environment around buildings. J. Wind Eng. Ind. Aerodyn. 96, 1749–1761.
Tominaga, Y., Mochida, A., Murakami, S., Sawaki, S., 2008b. Comparison of various revised k–ε models and LES applied to flow around a high-rise building model with 1: 1:2 shape placed within the surface boundary layer. J. Wind Eng. Ind. Aerodyn. 96 (4), 389–411.
Tominaga, Y., Stathopoulos, T., 2013. CFD simulation of near-field pollutant dispersion in the urban environment: a review of current modelling techniques. Atmos. Environ. 79, 716–730.
Tominaga, Y., Stathopoulos, T., 2016. Ten questions concerning modeling of near-field pollutant dispersion in the built environment. Build. Environ. 105, 390–402.
van Hooff, T., Blocken, B., 2010. Coupled urban wind flow and indoor natural ventilation modelling on a high-resolution grid: a case study for the Amsterdam ArenA stadium. Environ. Model. Softw. 25, 51–65.
Versteeg, H.K., Malalasekera, W., 2007. An Introduction to Computational Fluid Dynamics, second ed. Pearson Education, ISBN 978-0-13-127498-3.
Xie, Z., Coceal, O., Castro, I.P., 2008. Large-eddy simulation of flows over random urban like obstacles. Boundary-Layer Meteorol. 129, 1–23.
Xie, Z., Castro, I.P., 2006. LES and RANS for turbulent flow over arrays of wall-mounted obstacles. Flow. Turbul. Combust. 76, 291–312.